THE JOURNAL OF PHYSICAL CHEMISTRY A
A JOURNAL OF THE AMERICAN CHEMICAL SOCIETY

pubs.acs.org/JPCA

Article

Chemically Accurate Singlet−Triplet Gaps of Arylcarbenes from Local Hybrid Density Functionals

Published as part of The Journal of Physical Chemistry A virtual special issue "Gustavo Scuseria Festschrift".

Robin Grotjahn,* Justin Purnomo, Dayun Jin, Nicolas Lutfi, and Filipp Furche*

Cite This: *J. Phys. Chem. A* 2024, 128, 6046−6060

Read Online

ACCESS | Metrics & More | Article Recommendations | Supporting Information

ABSTRACT: Singlet−triplet (ST) gaps are key descriptors of carbenes, because their properties and reactivity are strongly spin-dependent. However, the theoretical prediction of ST gaps is challenging and generally thought to require elaborate correlated wave function methods or double-hybrid density functionals. By evaluating two recent test sets of arylcarbenes (AC12 and AC18), we show that local hybrid functionals based on the "common t" local mixing function (LMF) model achieve mean absolute errors below 1 kcal/mol at a computational cost only slightly higher than that of global hybrid functionals. An analysis of correlation contributions to the ST gaps suggests that the accuracy of the common t-LMF model is mainly due to an improved description of nondynamical correlation which, unlike exchange, is not additive in each spin-channel. Although spin-nonadditivity can be achieved using the local spin polarization alone, using the "common", i.e., spin-unresolved, iso-orbital indicator t for constructing the LMF is found to be critical for consistent accuracy in ST gaps of arylcarbenes. The results support the view of LHs as vehicles to improve the description of nondynamical correlation rather than sophisticated exchange mixing approaches.

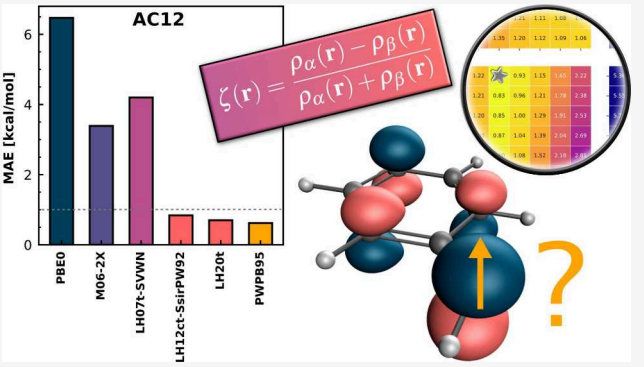

INTRODUCTION

Carbenes play an important role in organic synthesis, as ligands in transition metal complexes, or as intermediates in reaction mechanisms.[1−7] Carbenes are thought to be highly reactive due to a "sextet carbon" valence electron configuration. Their ground and low-lying excited states are prototypical examples of terms resulting from a two-electron two-orbital configuration; the two orbitals are energetically close, but not necessarily degenerate, and often conceptualized as a carbon sp^2 [although hybridization can vary] and a carbon p orbital (Figure 1). Although the triplet state is often the lowest energy state as in methylene, and may even be stabilized as in persistent triplet carbenes,[8,9] carbenes with singlet ground states also exist.[10] Singlet and triplet carbenes exhibit fundamentally different reactivities,[1,11] making accurate identification of the ground state critical.

The experimental determination of singlet−triplet (ST) gaps, $\Delta E_{ST} = E(T) - E(S)$, is notoriously difficult, making computational tools essential for both their prediction and validation. Theoretical contributions to the study of carbenes range from pioneering valence bond[12] or configuration interaction (CI)[13] studies on methylene and early density functional theory (DFT) calculations[14,15] to modern applications using higher-order coupled cluster methods[16] or DFT with multireference CI.[17] Recently, the domain-based pair natural orbital coupled-cluster singles doubles with perturbative triples [DLPNO−CCSD(T)] method[18−21] has been used in both applications[22,23] and to establish reference values for

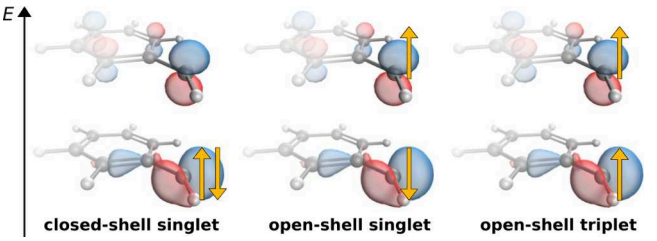

Figure 1. Schematic representation of the possible MO occupations and spin states in the simplest arylcarbene (phenylcarbene). The π-MO (p-like on the carbene center) is typically higher in energy than the σ-MO (sp^2-like). Arrows up (down) represent an electron with α (β) spin.

Received: April 30, 2024
Revised: June 21, 2024
Accepted: June 26, 2024
Published: July 16, 2024

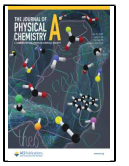

https://doi.org/10.1021/acs.jpca.4c02852
J. Phys. Chem. A 2024, 128, 6046−6060

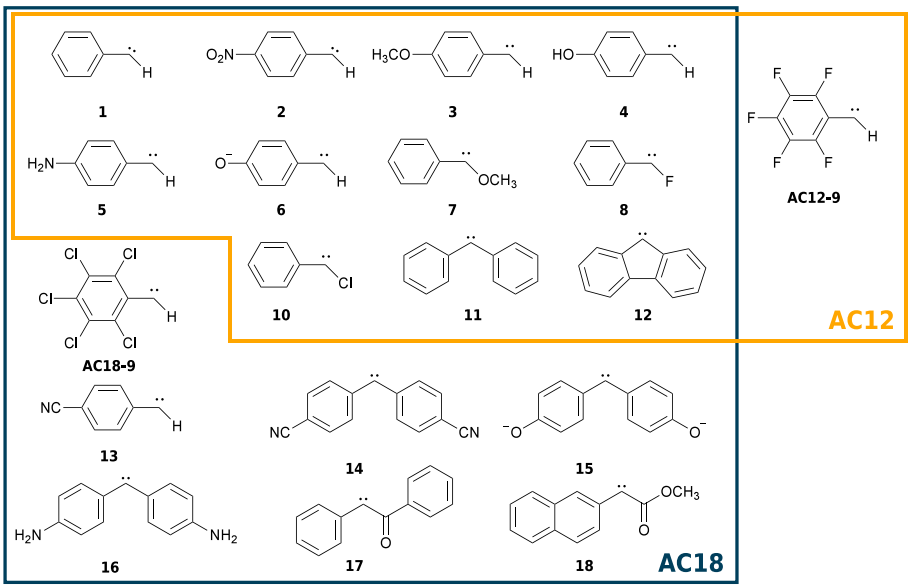

Figure 2. Lewis structures of the arylcarbenes from the AC12[24] and AC18[25] test sets evaluated in this work.

benchmark sets of arylcarbenes.[24,25] Arylcarbenes are of particular interest because spin delocalization (see Figure 1, top) can lead to stabilization of the triplet state.[9,24]

In ref 24, the AC12 set of ST gaps for 12 arylcarbenes was introduced (see Figure 2) along with canonical CCSD(T) reference values extrapolated to the complete basis set (CBS) limit by a [T/Q] extrapolation (molecules **1**−**10**) or a [D/T] extrapolation (molecules **11**−**12**). Comparison with other CC methods, including DLPNO methods, showed that DLPNO−CCSD(T)/CBS[T/Q] gives a mean absolute error (MAE) of 0.30 kcal/mol, while neglecting perturbative triples corrections as in DLPNO−CCSD/CBS[T/Q] leads to a slight deterioration with an MAE of 0.72 kcal/mol, which is, however, still within the 1 kcal/mol threshold for chemical accuracy. Canonical CCSD performs slightly worse with an MAE of 1.09 kcal/mol for molecules **1**−**10** at the CCSD/CBS[T/Q] level (vs 0.74 kcal/mol with the DLPNO method for the same molecules), indicating the possibility of some favorable error compensation. Among the six density functional approximations (DFAs) studied only the double hybrid (DH) functionals B2PLYP[26] and PWPB95[27] achieve chemical accuracy with MAEs of 0.87 and 0.62 kcal/mol, respectively, while the rung-4 global hybrid (GH) and semilocal functionals tested give much larger errors ranging from 2.19 kcal/mol (B3LYP[28−30]) to 5.91 kcal/mol (TPSSh[31]). A more detailed analysis of 17 DFAs for the adiabatic ST gaps in the 18 arylcarbenes of the AC18 test set[25] (see Figure 2) confirms these trends: While the DH mPW2PLYP[32,33] achieves close to chemical accuracy with an MAE of 1.10 kcal/mol, rung-4 hybrids including range-separated functionals such as ωB97X-D3[34,35] (3.13 kcal/mol) and highly parametrized functionals such as M06-2X[36] (4.04 kcal/mol) perform significantly worse.

To the best of our knowledge, local hybrid (LH) functionals[37−40] have not been evaluated for the ST gaps of arylcarbenes and the AC12/18 benchmarks. LHs use a local mixing function (LMF) to control the amount of exact-exchange (EXX) used in different parts of the system, aiming to fine-tune the delicate balance of self-interaction correction and nondynamical correlation.[41] LHs have evolved from simple models implemented in a post-SCF fashion[42−44] to well-performing functionals for thermochemistry and spectroscopy.[45−48] Initial problems for the implementation of LHs have been solved using efficient seminumerical integration techniques.[49−51] Here, we use the LH implementation in TURBOMOLE,[52,53] with support for ground state SCF[54] and gradients,[55] and excited states within time-dependent density functional theory (TDDFT).[56−60] Recently, range-separated local hybrids (RSLHs)[61] have been implemented in TURBOMOLE and have been shown to offer additional advantages, in particular by mitigating charge transfer errors.[47,62,63] LHs appear to be particularly promising for the prediction of ST gaps in arylcarbenes due to their exceptional performance for triplet excitation energies in TDDFT.[45,48,57,64−69] This has been linked to the use of a so-called common t-LMF, which leads to cross spin-channel terms for the local admixture of the EXX energy density and conversely for the nondynamical correlation energy (see Theory section).[67,69]

Here we present an assessment of (RS)LHs for ST gaps of arylcarbenes by evaluating their performance on the AC12 and AC18 test sets. Methylene, the simplest carbene, is studied alongside. To rationalize the good performance of certain LHs, model LMFs that explicitly depend on the spin polarization are constructed and analyzed. Similarities and differences in the real space dependence of the nondynamical energy density for different LHs in the methylene molecule provide further cues about the physical origin of the good performance of some LHs for triplet states.

THEORY

We write the spin-unrestricted LH exchange-correlation energy functional[70] as

$$E_{xc}^{LH}[\rho_\alpha, \rho_\beta] = E_x^{ex}[\rho_\alpha, \rho_\beta] + E_{NDC}^{LH}[\rho_\alpha, \rho_\beta] + E_c^{sl}[\rho_\alpha, \rho_\beta] \quad (1)$$

Here, $E_x^{ex}[\rho_\alpha, \rho_\beta]$ denotes the (unscaled) exact exchange energy functional, and $E_c^{sl}[\rho_\alpha, \rho_\beta]$ is a semilocal (sl) approximation to the correlation energy functional. The remainder,

https://doi.org/10.1021/acs.jpca.4c02852
J. Phys. Chem. A 2024, 128, 6046−6060

$$E_{\mathrm{NDC}}^{\mathrm{LH}}[\rho_\alpha, \rho_\beta] = \sum_\sigma \int \mathrm{d}^3 r[1 - a_\sigma(\mathbf{r})][e_{\mathrm{x},\sigma}^{\mathrm{sl}}(\mathbf{r}) - e_{\mathrm{x},\sigma}^{\mathrm{ex}}(\mathbf{r})] \tag{2}$$

is conventionally viewed as an "exchange mixing" term that replaces part or all of $E_{\mathrm{x}}^{\mathrm{ex}}$ with a sl approximation. In LHs, this is accomplished by a LMF $a_\sigma(\mathbf{r})$, which is a function of the local spin densities $\rho_\sigma(\mathbf{r})$ and other semilocal (sl) ingredients (see below). $e_{\mathrm{x},\sigma}^{\mathrm{ex}}(\mathbf{r})$ denotes the σ-spin exact Kohn−Sham exchange energy density which integrates to $E_{\mathrm{x}}^{\mathrm{ex}}$, and $e_{\mathrm{x},\sigma}^{\mathrm{sl}}(\mathbf{r})$ is a sl approximation to $e_{\mathrm{x},\sigma}^{\mathrm{ex}}(\mathbf{r})$, which integrates to the semilocal exchange energy $E_{\mathrm{x}}^{\mathrm{sl}}$. In the limit $a_\sigma(\mathbf{r}) = 1$, $E_{\mathrm{NDC}}^{\mathrm{LH}}$ vanishes, whereas for $a_\sigma(\mathbf{r}) = 0$, $E_{\mathrm{NDC}}^{\mathrm{LH}} = E_{\mathrm{x}}^{\mathrm{sl}} - E_{\mathrm{x}}^{\mathrm{ex}}$, thus replacing all of the exact exchange in $E_{\mathrm{xc}}^{\mathrm{LH}}$ with sl exchange. All these quantities are functionals of ρ_α and ρ_β, either explicitly, or implicitly through the occupied KS orbitals $\{\phi_{i\sigma}(\mathbf{r})\}$.

Among several LMF models (see ref 38 for a review), we focus on t-LMF models[37,43]

$$a_\sigma^{\mathrm{t}}(\mathbf{r}) = g t_\sigma(\mathbf{r}) \quad 0 < g \leq 1 \tag{3}$$

based on the iso-orbital indicator[71]

$$t_\sigma(\mathbf{r}) = \frac{\tau_{\mathrm{W},\sigma}(\mathbf{r})}{\tau_\sigma(\mathbf{r})} \tag{4}$$

which compares the σ-spin von-Weizsäcker kinetic energy density

$$\tau_{\mathrm{W},\sigma}(\mathbf{r}) = \frac{1}{2}|\nabla\sqrt{\rho_\sigma(\mathbf{r})}|^2 \tag{5}$$

to its Kohn−Sham equivalent

$$\tau_\sigma(\mathbf{r}) = \frac{1}{2}\sum_i^N |\nabla\phi_{i,\sigma}(\mathbf{r})|^2 \tag{6}$$

If one takes the conventional view of $E_{\mathrm{NDC}}^{\mathrm{LH}}[\rho_\alpha, \rho_\beta]$ as an "exchange mixing" functional, then the spin scaling relation[72]

$$E_{\mathrm{x}}[\rho_\alpha, \rho_\beta] = \frac{1}{2}(E_{\mathrm{x}}[2\rho_\alpha] + E_{\mathrm{x}}[2\rho_\beta]) \tag{7}$$

where $E_x[\rho]$ is the closed-shell or spin-unpolarized exchange energy, dictates that the LMF for σ-spin exchange depend solely on σ-spin quantities. The resulting model for $E_{\mathrm{NDC}}^{\mathrm{LH}}[\rho_\alpha, \rho_\beta]$ satisfies eq 7 and is thus additive in each spin-channel.

However, as discovered in ref 67 and discussed in more detail in ref 69, the description of triplet excitation energies in TDDFT can be significantly improved by introducing the "common t-LMF"[70]

$$a_\sigma^{\mathrm{ct}}(\mathbf{r}) = a^{\mathrm{ct}}(\mathbf{r}) = g\frac{\tau_W(\mathbf{r})}{\tau_\alpha(\mathbf{r}) + \tau_\beta(\mathbf{r})} \tag{8}$$

which is independent of σ, because it depends on

$$\tau_{\mathrm{W}}(\mathbf{r}) = \frac{1}{2}|\nabla\sqrt{\rho(\mathbf{r})}|^2 \tag{9}$$

where $\rho(\mathbf{r}) = \rho_\alpha(\mathbf{r}) + \rho_\beta(\mathbf{r})$ denotes the *total* density. The use of the spin-unresolved quantity τ_{W}/τ instead of t_σ was pioneered by Tao, Perdew, Staroverov, and Scuseria,[73] who employed it to impose correct spin-dependence of the TPSS *correlation* energy functional in the low density limit. Indeed, $E_{\mathrm{NDC}}^{\mathrm{LH}}[\rho_\alpha, \rho_\beta]$ is no longer additive in the two spin-channels within the common t-LMF model, in apparent violation of eq 7. A continuous interpolation between the same spin-channel t-LMF a_σ^{t}, the common LMF a_σ^{ct}, and the opposite spin-channel t-LMF[74]

$$a_\sigma^{\mathrm{ot}}(\mathbf{r}) = g t_{\sigma'}(\mathbf{r}) \tag{10}$$

with σ' indicating the spin-channel opposite to σ, was proposed in ref 69,

$$a_\sigma^{\mathrm{smt}}(\mathbf{r}) = \frac{g}{2}\frac{|\nabla\sqrt{m\rho_\sigma(\mathbf{r}) + (1-m)\rho_{\sigma'}(\mathbf{r})}|^2}{m\tau_\sigma(\mathbf{r}) + (1-m)\tau_{\sigma'}(\mathbf{r})} \tag{11}$$

where the empricial parameter m satisfies $0 \leq m \leq 1$. This interpolation is designed such that

$$a_\sigma^{\mathrm{smt}}(\mathbf{r}) = \begin{cases} a_\sigma^{\mathrm{t}}(\mathbf{r}); & m = 1 \\ a_\sigma^{\mathrm{ct}}(\mathbf{r}); & m = 0.5 \\ a_\sigma^{\mathrm{ot}}(\mathbf{r}); & m = 0 \end{cases} \tag{12}$$

An analysis of 105 singlet and 105 triplet excitation energies showed that triplet excitation energy errors are systematically reduced as m decreases from 1 to 0.5, introducing opposite spin dependence in the LMF.[69] Beyond $m = 0.5$, any further improvements were miniscule.

We also aim to understand whether and to what extend this approach is consistent with the original idea of local hybrids,[38] i.e., using more exact exchange in one-electron regions to reduce self-interaction errors while approximating nondynamical correlation by the semilocal exchange functional in other regions. In fact, information from the opposite spin-channel could be included in the LMF in a more straightforward way than in the usual common t-LMF by using the local spin polarization

$$\zeta(\mathbf{r}) = \frac{\rho_\alpha(\mathbf{r}) - \rho_\beta(\mathbf{r})}{\rho_\alpha(\mathbf{r}) + \rho_\beta(\mathbf{r})} \tag{13}$$

To treat the α and β spin-channels on an equal footage, the squared spin polarization ζ^2 is used, which varies between 0 and 1. LMFs with explicit dependence on the spin polarization are not a new idea per se and have been reported before.[74−78] However, to the best of our knowledge, their performance for triplet states or ST gaps has not been analyzed. As a model to study the importance of the spin polarization as an ingredient in the LMF, we consider the spin polarization (squared) t-LMF (spqt-LMF)

$$a_\sigma^{\mathrm{spqt}}(\mathbf{r}) = g[1 - m\zeta^2(\mathbf{r})][b t_\sigma(\mathbf{r}) + (1-b)] \tag{14}$$

where $0 \leq m \leq 1$ interpolates between the weakest and strongest influence of the spin polarization, $0 \leq b \leq 1$ interpolates between a constant LMF and a spin-channel t-LMF, and $0 < g \leq 1$ is a global scaling factor. This model allows us to study the effects of the spin-polarization real-space dependence of the LMF (parameter m) independently from those of the iso-orbital indicator real-space dependence of the LMF (parameter b). A particularly interesting limit is $b = 0$, where the spqt-LMF reduces to the spq-LMF

$$a_\sigma^{\mathrm{spq}}(\mathbf{r}) = g[1 - m\zeta^2(\mathbf{r})] \tag{15}$$

for a triplet state and to $a_\sigma^{\mathrm{spq}}(\mathbf{r}) = g$ for a singlet state. That is, for a triplet state, the real-space dependence of the LH is determined solely by the spin polarization term, whereas for a singlet state the LH effectively becomes a GH with a mixing factor g. The spqt-LMF was implemented in a developer's

https://doi.org/10.1021/acs.jpca.4c02852
J. Phys. Chem. A 2024, 128, 6046−6060

version of TURBOMOLE.[52,53,79] To enable SCF and linear-response TDDFT calculations, the first and second partial derivatives with respect to the semilocal quantities were implemented and checked against finite difference results for ground state gradients and static polarizabilities of open-shell systems.

COMPUTATIONAL DETAILS

All calculations were performed using a developer's version of TURBOMOLE V7.8.[52,53,79] We studied the predefined local hybrids LH07t-SVWN,[43] LH07s-SVWN,[42] LH12ct-SsirPW92,[70] LH12ct-SsifPW92,[70] LH14t-calPBE,[80] LH20t,[45] TMHF,[81] TMHF-3P,[81] and LH23pt,[48] as well as the range-separated local hybrids ωLH22t,[47] and ωLH23ct-sir[63] (all included in the official V7.8 release). In addition, the semilocal functionals PBE,[82] BLYP,[29,83] TPSS,[73] SCAN,[84] r^{2}SCAN,[85] and M06-L,[86] the global hybrids TPSSh,[31] B3LYP,[28−30] PBE0,[82,87] SCAN0,[88] and M06-2X,[36] as well as the range-separated global hybrids CAM-B3LYP,[89] ωB97X-D3,[34,35] and ωB97M-V[90] were studied for comparison. As indicated by a suffix to the functional name, in some calculations dispersion effects have been taken into account using semiempirical DFT-D3,[91] DFT-D3(BJ) with Becke-Johnson damping,[92] or DFT-D4[93−95] corrections.

The ST gaps were calculated in an adiabatic ΔSCF approach

$$\Delta E_{ST} = E_{UKS}(T\,//\,T) - E_{RKS}(S\,//\,S) \tag{16}$$

using the unrestricted KS (UKS) formalism for the triplet state (at the triplet state structure) and the restricted Kohn−Sham (RKS) formalism for the singlet state (at the singlet state structure). The singlet and triplet state structures were kept fixed at the reference structure (AC12 test set) or relaxed with the respective functional studied (AC18 test set). For the AC12 and AC18 benchmark sets, the stability of the RKS singlet solutions was confirmed by the calculation of the lowest eigenvalue of the singlet instability Hessian. Additional test calculations with the LH20t functional for the spin-symmetry broken open-shell singlet states of the AC12/18 test sets confirmed that the closed-shell singlet states are lower in energy. Although open-shell singlet states are inherently multideterminantal, their energies and densities are often captured reasonably well by spin-symmetry broken UKS solutions.[96−98]

Methylene. Structure optimizations for methylene used cc-pVTZ[99] basis sets. For better comparability, the ST gaps were obtained from single point calculations using cc-pV6Z basis sets[100,101] on the CCSD(T)/cc-pVTZ structures reported in ref 24. Very fine quadrature grids (TURBOMOLE gridsize 5) were used. Potential energy surface (PES) scans used def2-QZVPD[102,103] basis sets and fine quadrature grids (TURBOMOLE gridsize 4). The C−H bond lengths were sampled from 0.95 to1.29 Å in 0.01 Å increments and the bond angle was sampled from 86 deg to 170 deg in 2 deg increments.

AC12 Test Set. For consistency with ref 24, all calculations were performed as single-point calculations using the B3LYP-D3(BJ)/def2-TZVPP structures from ref 24, def2-TZVPP basis sets,[104] and the resolution of the identity (RI) approximation[105] for the Coulomb part together with def2-TZVPP[106] fitting basis sets. Fine quadrature grids (TURBOMOLE gridsize 4) were used for all XC functionals except SCAN and SCAN0, where finer grids were used to ensure grid convergence (TURBOMOLE reference grid, radsize 50).

AC18 Test Set. For consistency with ref 25, all calculations used the following protocol: First, the singlet and triplet state structures were optimized with the respective functional using def2-TZVPP basis sets, fine quadrature grids (TURBOMOLE gridsize 4), quadrature weight derivatives, the RI approximation, and a convergence threshold of 10^{-4} a.u. for the gradient norm. With these structures, ST gaps were obtained from single-point calculations without the RI approximation using def2-QZVPP basis sets and fine quadrature grids (TURBOMOLE gridsize 4).

Transferability to TDDFT. The performance of LHs based on the spqt-LMF was assessed for the vertical singlet and triplet excitation energies of the QUEST-ST test set, which is a subset of the QUEST test set,[107] devised in ref 69 that considers pairs of singlet and triplet excitations that are identical in their orbital character and only differ in their multiplicity. The computational details are unchanged from ref 69 (aug-cc-pVTZ basis sets,[99,108] TURBOMOLE gridsize 3, no RI). The following 26 singlet and 26 triplet states were dropped from the final statistical evaluation to avoid difficulties in the state assignment as the dominant orbital character of the singlet and/or triplet excitation changed upon varying b, m, and/or g in the spqt-LMF: 5, 7, 9, 20, 22, 24, 25, 30, 31, 35, 42, 48, 52, 56, 57, 58, 63, 64, 67, 69, 74, 81, 82, 87, 102, 111 (numbering as in ref 69). While more elaborate excited state assignment schemes could be used instead, the remaining 79 singlet and 79 triplet states (75.2% of the original test set size) seemed sufficient for our purpose of confirming that the spqt-LMF behaves similarly for TDDFT excitation energy calculations as it does for adiabatic ΔSCF calculations of ST gaps.

BENCHMARK RESULTS

Methylene. The methylene molecule has been extensively studied experimentally.[109,110] Its small system size has allowed the authors of ref 24 to perform calculations with the iterative configuration expansion configuration interaction (ICE-CI) method[111,112] to obtain a cc-pV[T/Q]Z basis set extrapolated correlation energy, which was added to the cc-pV6Z HF result, giving a very good approximation of the full-CI complete basis set result for the ST gap of −9.19 kcal/mol (Table 1). All the XC functionals studied give the correct qualitative trends for the equilibrium structures of the singlet and triplet states: The C−H bond length is shortened and the bond angle is widened in the triplet state compared to the singlet. The signs for the ST gaps are also correctly reproduced, with all functionals predicting the triplet state to be lower in energy. While the numerical differences for the structural parameters are rather subtle, the ST gaps is significantly underestimated with all global hybrids with both nonempirical (TPSSh, PBE0) functionals and (semi)empirical (B3LYP, M06-2X) functionals. The best agreement with the ICE-FCI data is obtained with the GGA BLYP, the local hybrids LH12ct-SsifPW92 and LH20t, and the range-separated hybrid ωB97M-V (Table 1). While the perfect numerical agreement of the LH12ct-SsifPW92 functional with the reference data is coincidental, this provides some preview of the results to be presented below for the more extensive AC12/18 test sets. Considering also the structural parameters, ωB97M-V gives the worst agreement for the triplet state bond angle among the studied functionals while LH12ct-SsifPW92 and LH20t come much closer to the experimental reference value. While the agreement of the ST gap predicted with BLYP is remarkable, the singlet bond angle

https://doi.org/10.1021/acs.jpca.4c02852
J. Phys. Chem. A 2024, 128, 6046−6060

Table 1. Structural Parameters[a] and Singlet−Triplet Gap (kcal/mol) for Methylene[b]

	Singlet		Triplet		
Method	R (C−H)	θ	R (C−H)	θ	ΔE_{ST}
Reference	1.107[c]	102.4[c]	1.075[d]	133.9[d]	−9.19[e]
CCSD(T)[f]	1.111	101.6	1.108	133.5	−9.50
BLYP	1.101	114.0	1.084	135.4	−9.65
TPSSh	1.115	101.4	1.080	135.1	−17.29
B3LYP	1.111	101.6	1.078	135.0	−10.87
PBE0	1.113	101.4	1.078	134.7	−16.70
M06-2X	1.107	101.8	1.076	134.2	−13.20
ωB97X-D	1.109	101.8	1.079	134.2	−11.41
ωB97M-V	1.108	101.4	1.076	136.1	−8.41
LH12ct-SsifPW92	1.111	102.6	1.081	134.8	−9.19
LH20t	1.103	103.1	1.074	134.6	−8.29

[a]Bond lengths in Å, angles in deg. [b]Structure optimizations used cc-pVTZ basis sets, singlet-triplet gaps were obtained from single point calculations using cc-pV6Z basis sets on CCSD(T)/cc-pVTZ structures. [c]Experimental data from ref 109. [d]Experimental data from ref 110. [e]ICE-FCI/cc-pV6Z results from ref 24 obtained by a two-point [T,Q] basis set extrapolation of the correlation energy. [f]Results from ref 24. ΔE_{ST} values are basis set extrapolated as explained in footnote e above.

is significantly overestimated. We will return to the good performance of BLYP for ST gaps below.

We also performed a scan of the PES of methylene considering the closed-shell singlet, the open-shell singlet, and the triplet state selecting LH12ct-SsifPW92 as an example of a local hybrid and PBE0 as a global hybrid. The results are included in the Supporting Information (Figure S1). Notably, the minimum of the UKS singlet PES is lower than the RKS singlet minimum with PBE0 but higher in energy with LH12ct-SsifPW92. This seems to be related to the degree to which these two functionals suffer from spin contamination. Averaged over all geometries sampled for the PES, LH12ct-SsifPW92 gives an $\langle S^2 \rangle$ expectation value of 2.0063 for the triplet state, i.e., a spin contamination of 0.0063 with a maximum spin contamination of up to 0.0169 at the most extremely distorted geometry (θ = 170 deg, R(C−H) = 1.29 Å). With PBE0, the average spin contamination is larger (0.0792) and reaches up to 0.0225. These trends transfer to the spin symmetry broken UKS singlet state where the average $\langle S^2 \rangle$ expectation value is 1.0030 for LH12ct-SsifPW92 and 1.0056 for PBE0.

AC12 Test Set: ST Gaps at Fixed Structures. The statistical results for the AC12 test set of ref 24 are presented in Table 2 and Figure 3; individual ST gaps for all 12 molecules are reported in the Supporting Information (Table S1). With most nonhybrids, GHs, RSHs, and some LHs, the ST gaps are underestimated with MSEs of ca. −4 kcal/mol. This relative overstabilization of the triplet state is reminiscent of the triplet problem of TDDFT[113] and commonly observed in hybrid TDDFT calculations. ωB97M-V is a notable exception with an MSE of +1.04 kcal/mol.

Surprisingly, with an MAE of only 1.29 kcal/mol, the GGA BLYP performs significantly better than PBE (4.12 kcal/mol). Additional calculations with the B88-PBE (4.76 kcal/mol) and PBE-LYP (1.19 kcal/mol) functionals indicate that the LYP correlation functional is responsible for the remarkable performance of this GGA functional for the present data set. The LYP functional features a reduced amount of parallel spin correlation approaching zero for the case of systems in which all spins are aligned.[29] For the systems studied here, the removal of (negative) correlation energy for the triplet state increases its energy relative to the singlet state, thus mitigating the underestimation of the ST gap observed with other GGAs such as PBE. Considering also the poor performance of BLYP for the bond angle of the singlet state in methylene (see above), this effect is probably best viewed as a favorable error compensation that is not guaranteed to transfer to other sets of systems. Revisiting a test set of 23 S_1-T_1 gaps from the QUEST database[107] reported by one of us in ref 69, we find that BLYP also performs remarkably well in these TDDFT calculations with an MAE of 0.25 eV (PBE0:0.42 eV). However, this subset has been deliberately biased toward systems where the orbital characters of the singlet and triplet states are identical, thus facilitating error compensation effects. Reanalysis of the S_1-T_1 gaps for the singlet fission chromophores of ref 64 as well as the S_1-T_1 gaps reported for the Thiel test set[114] in ref 67 show no advantages for the BLYP functional.

The meta-GGA SCAN and its regularized version r^{2}SCAN perform significantly worse than their meta-GGA predecessor TPSS or their GGA predecessor PBE with their MAEs more than doubled. Evidently, the strong focus in the construction of the SCAN exchange functional to resemble the behavior of exact exchange resulting in an improved description of localized XC holes[84] has an adverse effect on the prediction of ST gaps in arylcarbenes. The behavior of SCAN to resemble global hybrid functional behavior has also been shown for TDDFT excitation energies and the triplet instability problem.[115] This is somewhat unexpected as SCAN was shown to capture the energetics of strong correlation for challenging systems such as the C_2 dimer when allowing spin-symmetry breaking.[116] The problem is further aggravated for the SCAN based global hybrid SCAN0 (25% EXX). Similar to the case of PBE and PBE0, SCAN0 falls further behind the pure SCAN functional, indicating that controlling self-interaction errors is not an effective strategy for reducing errors in arylcarbene ST gaps, whether through global EXX admixture or improved semilocal exchange holes.

The local hybrids based on a common t-LMF, i.e., LH12ct-SsirPW92, LH12ct-SsifPW92, and LH20t, all give MAEs below 1 kcal/mol with narrow error distributions and maximum errors not exceeding ±1.7 kcal/mol. The MSEs are close to 0, indicating little remaining systematic error for these functionals. LH20t outperforms the DH B2PYLP and is on a par with the DH PWPB95 and the DLPNO−CCSD method. The recent LH23pt functional,[48] which uses a density-based Padé form to modify the common t-LMF, especially in the core region and asymptotics, also performs well, albeit with a slightly negative MSE. While still performing well compared to most GHs, the range-separated LH ωLH22t underestimates all ST gaps with an MAE of 1.86 kcal/mol. The recent ωLH23ct-sir functional,[63] which is designed to restore the good performance for triplet excitation energies in TDDFT known from LHs also for RSLHs, significantly improves the ST gaps of the AC12 test set compared to ωLH22t, giving an MAE of 1.12 kcal/mol.

Although we have included semiempirical dispersion corrections in many of the calculations, their effect is actually negligible, as can be seen by comparing the results of LH20t, LH20t-D3(BJ), and LH20t-D4. The largest effect is found for molecule **11** (diphenylmethylene), with a change in the ST gap of +0.31 kcal/mol when including the -D4 dispersion corrections (Table S1 in the Supporting Information).

https://doi.org/10.1021/acs.jpca.4c02852
J. Phys. Chem. A 2024, 128, 6046−6060

Table 2. Error Statistics for the AC12 Test Set (kcal/mol)[a]

Method	MaxE(+)	MaxE(−)	MSE	RMSE	MAE
PBE-D3(BJ)	−1.94	−6.19	−4.12	4.35	4.12
BLYP-D3(BJ)	0.99	−3.92	−0.75	1.66	1.29
M06-L-D3	−3.06	−7.80	−5.19	5.35	5.19
TPSS-D3(BJ)	−3.19	−6.57	−5.00	5.13	5.00
SCAN-D3(BJ)[b]	−8.24	−13.84	−11.42	11.55	11.42
SCAN[b]	−8.25	−13.85	−11.44	11.57	11.44
r^{2}SCAN	−7.95	−11.45	−9.66	9.74	9.66
TPSSh-D3(BJ)	−4.55	−7.44	−5.90	5.97	5.90
B3LYP-D3(BJ)	−0.61	−4.27	−2.23	2.47	2.23
PBE0-D3(BJ)	−5.00	−7.77	−6.47	6.53	6.47
SCAN0[b]	−11.37	−15.91	−13.89	13.98	13.89
M06-2X-D4	−2.54	−4.54	−3.39	3.45	3.39
CAM-B3LYP-D3(BJ)	−1.90	−4.29	−3.31	3.38	3.31
ωB97X-D3	−1.84	−4.12	−3.04	3.12	3.04
ωB97M-V	1.93	−0.30	1.04	1.21	1.09
LH07t-SVWN-D3	−2.81	−5.80	−4.20	4.29	4.20
LH07s-SVWN-D3	−3.12	−5.93	−4.49	4.58	4.49
LH14t-calPBE-D3	−3.45	−6.36	−4.71	4.77	4.71
TMHF	−1.44	−4.55	−3.19	3.32	3.19
TMHF-3p	−1.74	−4.58	−3.48	3.58	3.48
LH12ct-SsirPW92-D3	1.59	−1.56	0.00	0.96	0.84
LH12ct-SsifPW92-D3	1.66	−1.55	0.04	0.98	0.87
LH20t	1.64	−1.24	0.11	0.83	0.68
LH20t-D3(BJ)	1.65	−1.22	0.13	0.83	0.70
LH20t-D4	1.67	−1.21	0.15	0.84	0.71
LH23pt-D4	0.37	−2.39	−1.06	1.31	1.12
ωLH22t-D4	−0.71	−2.84	−1.86	1.96	1.86
ωLH23ct-sir	0.17	−2.27	−1.10	1.33	1.12
B2PLYP-D[c,d]	2.81	−1.06	0.60	1.14	0.87
PWPB95-D[c,d]	1.39	−0.51	0.30	0.73	0.62
DLPNO−CCSD/CBS[T/Q][c]	−0.08	−1.25	−0.72	0.81	0.72
DLPNO−CCSD(T)/CBS[T/Q][c]	0.43	−1.05	0.01	0.40	0.30

[a]Errors are given wrt. the canonical CCSD(T)/CBS reference values from ref 24. All calculations were performed as single-point calculations on B3LYP-D3(BJ)/def2-TZVPP structures.[24] DFT calculations used def2-TZVPP basis sets. [b]Finer quadrature grid settings were used (see Computational Details). [c]Results from ref 24. [d]With Grimme's dispersion corrections (version not specified in ref 24).

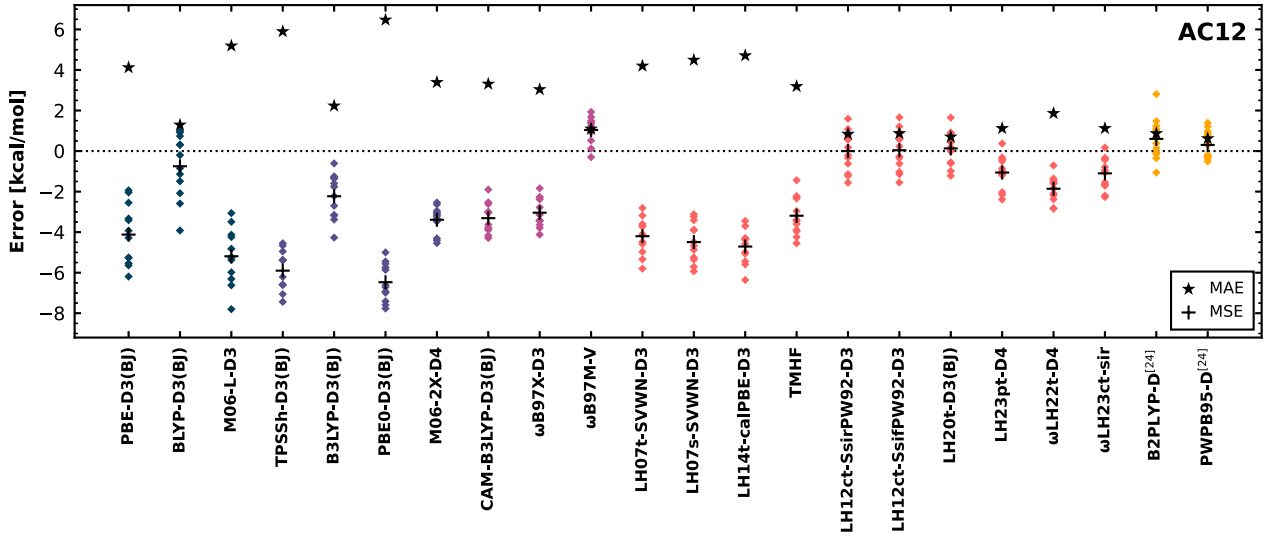

Figure 3. Scatter plots of the signed errors for the ST gaps of the AC12 test set with respect to the canonical CCSD(T)/CBS reference values from ref 24. All calculations were performed as single-point calculations on B3LYP-D3(BJ)/def2-TZVPP structures.[24] DFT calculations used def2-TZVPP basis sets. Results for double hybrids are taken from ref 24 and include dispersion corrections (version not specified).

https://doi.org/10.1021/acs.jpca.4c02852
J. Phys. Chem. A 2024, 128, 6046−6060

AC18 Test Set: ST Gaps at Optimized Structures. Overall, the quality of the reference data for the AC18 test set of ref 25 is somewhat lower than for the AC12 set because AC18 relies on basis set extrapolated DLPNO−CCSD(T1) energies as opposed to canonical CCSD(T) for AC12. For the AC12 set, the DLPNO results differ from the canonical results by 0.3 kcal/mol on average, but individual errors can be as large as −1.05 kcal/mol (Table 2 and ref 24). Furthermore, the evaluation of the AC18 test set is based on method-specific structure optimization for the DFT methods and OO-SCS-MP2 reference geometries for the DLPNO−CCSD(T1) energies. While this also introduces some ambiguity in explaining the origin of the error patterns, a protocol with method-specific optimization is also closer to how DFT would be used in practical applications. The slightly larger sample size of AC18 and the large system sizes of some of its members also make it an interesting extension.

The statistical results for the AC18 test set are presented in Table 3 and Figure 4; individual ST gaps for all 18 molecules

Table 3. Error Statistics (kcal/mol) for the AC18 Test Set[a]

Method	MaxE(+)	MaxE(−)	MSE	RMSE	MAE
PBE-D3(BJ)[b]	3.19	−6.65	−3.19	3.95	3.54
BLYP-D3BJ[b]	5.31	−4.42	−0.17	2.19	1.68
M06-L[b]	−1.07	−8.53	−5.02	5.29	5.02
TPSSh-D3BJ[b]	−1.20	−7.72	−5.24	5.49	5.24
B3LYP-D3(BJ)[b]	1.87	−4.66	−1.76	2.32	1.97
PBE0-D3(BJ)[b]	−2.31	−8.25	−6.08	6.29	6.08
M06-2X[b]	−1.83	−5.35	−4.04	4.14	4.04
CAM-B3LYP-D3(BJ)	−0.02	−4.53	−3.36	3.54	3.36
ωB97X-D3[b]	−0.02	−4.34	−3.13	3.34	3.13
ωB97M-V	3.57	−0.79	0.85	1.23	0.99
LH07t-SVWN-D3	0.27	−6.17	−3.99	4.27	4.02
LH07s-SVWN-D3	0.37	−6.54	−4.11	4.42	4.15
LH14t-calPBE	−0.56	−6.68	−4.50	4.71	4.50
TMHF	−0.25	−4.91	−3.13	3.32	3.13
TMHF-3p	−0.51	−4.90	−3.41	3.59	3.41
LH12ct-SsirPW92-D3	3.29	−2.24	0.00	1.30	1.05
LH12ct-SsifPW92-D3	3.36	−2.26	0.04	1.31	1.06
LH20t	2.44	−1.87	−0.05	1.06	0.88
LH20t-D3(BJ)	2.80	−1.85	0.04	1.11	0.90
LH23pt	1.59	−2.70	−1.12	1.53	1.33
ωLH22t-D3(BJ)	1.14	−3.09	−1.71	1.95	1.84
ωLH23ct-sir	1.91	−4.03	−1.48	1.97	1.70
B2PLYP-D3[b]	4.58	−1.60	1.10	1.97	1.53
mPW2PLYP[b]	3.24	−2.03	0.29	1.38	1.09

[a]Errors are given wrt. the cc-pV[T/Q]Z basis set extrapolated DLPNO−CCSD(T1) references values from ref 25 obtained at OO-SCS-MP2 geometries. DFT calculations were performed by method specific optimization (def2-TZVPP basis sets) followed by single-point calculations (def2-QZVPP basis sets). [b]Results from ref 25.

are reported in the Supporting Information (Table S2). Overall, the trends in the MAEs and MSEs are very similar to those found for the AC12 test set (see Table 2). To some extent, this was to be expected given the considerable overlap between the two sets of 11/18 molecules. It also shows that method-specific geometry optimization does not dramatically affect the performance of the functionals studied. The comparatively small effect of the equilibrium structure on adiabatic energy gaps is also well-known, e.g. for adiabatic excitation energies from TDDFT.[117] A comparison of Figure 3 and Figure 4 shows wider error distributions for the AC18 test set. For many functionals, molecule **17** is an outlier from the remaining data points. As discussed in ref 25, this may be due to a significant error in the carbene bond angle of 10.47 deg with the OO-SCS-MP2 method, which serves as the reference geometry for the DLPNO−CCSD(T1) single point calculations.

Although ωB97M-V also performs exceptionally well on average with an MAE of 0.99 kcal/mol, it systematically overestimates the ST gaps and shows a significant outlier with an error of +3.57 kcal/mol (molecule **17**), while LH20t gives a slightly lower MAE, shows essentially no systematic error with an MSE of −0.05 kcal/mol, and gives a maximum error of +2.44 kcal/mol (also for molecule **17**).

■ ANALYSIS

A series of formal analyses for the AC12 set and the methylene molecule is performed to understand the good performance of some LHs for the ST gaps of carbenes. First, it is shown that the good performance of common t-LMF based LHs such as LH20t and LH12ct-SsirPW92 compared to spin-channel t-LMF based LHs is linked to the middle-term in eq 1. Next, we show that similar advantages are achieved by the "brute-force" inclusion of the opposite spin-channel in the LMF via the spq(t)-LMF models (eq 14, eq 15). Further comparison of the spq-LMF and spqt-LMF elucidate the importance of the iso-orbital indicator for the performance of LHs for ST gaps.

Energy Decomposition. Following Perdew and co-workers,[75] we consider $E_{\mathrm{NDC}}^{\mathrm{LH}}$ an approximation to the exact nondynamical (or static) correlation energy functional defined by

$$E_{\mathrm{NDC}}[\rho_\alpha, \rho_\beta] = E_{\mathrm{c}}[\rho_\alpha, \rho_\beta] - E_{\mathrm{c}}^{\mathrm{sl}}[\rho_\alpha, \rho_\beta] \tag{17}$$

The sl correlation energy functional is viewed as purely dynamical, i.e., $E_{\mathrm{DC}}[\rho_\alpha, \rho_\beta] = E_{\mathrm{c}}^{\mathrm{sl}}[\rho_\alpha, \rho_\beta]$, because the semilocal correlation hole is short-ranged and typically does not capture static correlation in finite systems caused by near-degeneracy effects. The total LH energy functional can thus be decomposed as

$$E_{\mathrm{total}}^{\mathrm{LH}}[\rho_\alpha, \rho_\beta] = E_{\mathrm{HFKS}}[\rho_\alpha, \rho_\beta] + E_{\mathrm{NDC}}^{\mathrm{LH}}[\rho_\alpha, \rho_\beta] + E_{\mathrm{DC}}[\rho_\alpha, \rho_\beta] \tag{18}$$

where E_{HFKS} is the energy expectation value of the KS determinant. Even though the models for E_{NDC} considered here exhibit exchange-like behavior under uniform scaling of the total density and thus are best viewed as "rung 3.5" functionals,[39,118] the spin-nonadditivity of our model for E_{NDC} is a characteristic of (static) correlation and arguably more important for ST gaps than uniform scaling of the total density, whose extent is relatively similar for the lowest singlet and triplet state in carbenes.

The contributions of each term in eq 18 to the ST gaps of the AC12 test set were analyzed for a common t-LMF and a spin-channel t-LMF based LH. The results shown in Figure 5 reveal the effects of the common LMF as the difference between the squares and circles (solid and dashed lines). While each individual data series is obtained as the difference of the singlet and triplet energies, comparing the common and spin-channel LMF series simplifies to comparing the changes in the triplet state energies as singlet states are described equally by both LMF models (cf. eq 8) and eq 3. The data series for the total energies (yellow) are consistent with the observation that,

https://doi.org/10.1021/acs.jpca.4c02852
J. Phys. Chem. A 2024, 128, 6046−6060

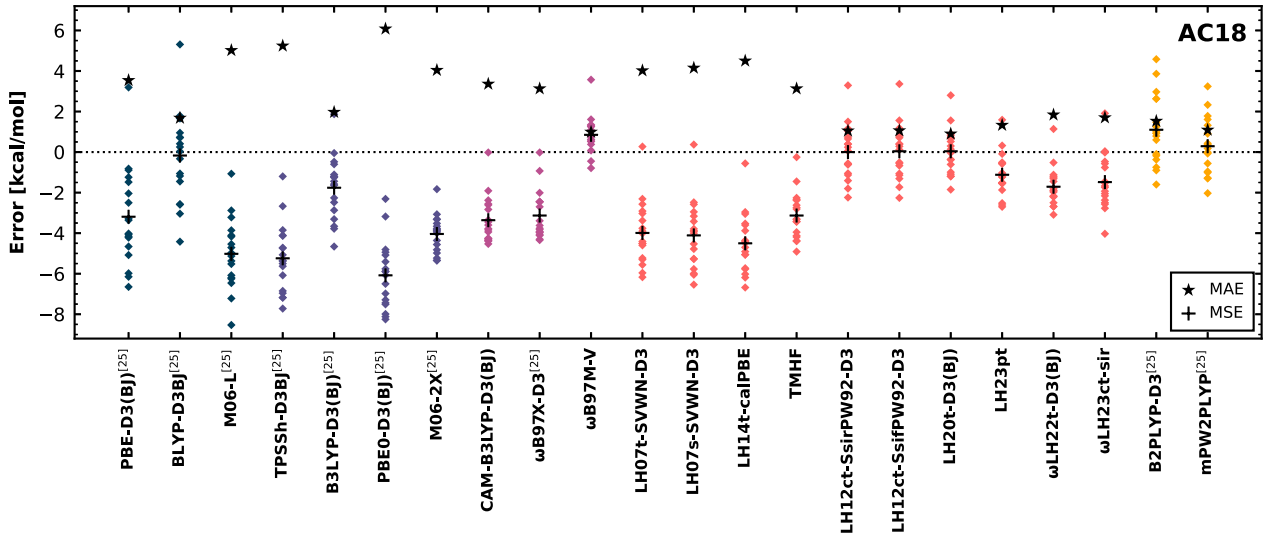

Figure 4. Scatter plots of the signed errors for the ST gaps of the AC18 test set wrt. the cc-pV[T/Q]Z basis set extrapolated DLPNO−CCSD(T1) references values from ref 25 obtained at OO-SCS-MP2 geometries. DFT calculations were performed by method specific optimization (def2-TZVPP basis sets) followed by single-point calculations (def2-QZVPP basis sets). Some results from ref 25 are included for comparison.

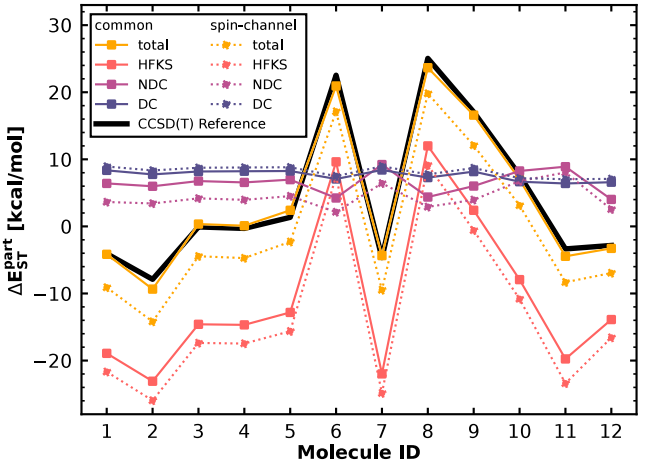

Figure 5. Decomposition of the differences in energy of the T_1 and S_0 states for the 12 molecules from the AC12 test set into different contribution to the total energy difference (ST gap). Results with a common t-LMF (eq 8) based LH-ct0.709-SsifPW92 functional (squares) are compared against results with a spin-channel t-LMF (eq 3) based LH-t0.709-SsifPW92 functional (circles). Connecting lines are added for visual clarity.

on average, the spin-channel t-LMF based LHs underestimate the ST gaps considerably while many common t-LMF based LHs give excellent agreement with the reference values. The small changes in the dynamical correlation energy data series (purple) are merely a consequence of changes in the self-consistent orbitals caused by other components of the LH potential, since the definition of $E_{DC} = E_c^{sl}$ does not change when going from a spin-channel to a common LMF. Most of the changes in the total energy data series are explained by changes in the NDC (pink) and HFKS (red) energies with similar contributions from both parts. Notably, the trends for the differences between the spin-channel and common LMF are very systematic, while the individual contributions to the ST gap vary significantly in magnitude and, in some cases sign, among the molecules in the AC12 test set. This strongly discourages the possibility of favorable stochastic error compensation by virtue of the limited size of the test set. Additional calculations with the VWN correlation functional and without a correlation functional show that these trends are independent of choice of the correlation functional (Figure S2).

Explicitly Spin Polarization Dependent LMFs Compared to Common LMFs. To show that the good performance of common t-LMF based LHs for the AC12 test set is indeed linked to the common t-LMF's inclusion of information on the opposite spin-channel, simpler explicitly spin-polarization dependent LMFs (the spqt-LMF (b = 1) and the spq-LMF) are analyzed for different values of the spin-polarization prefactor m and compared to the smt-LMF that reduces to the common LMF for a spin mixing parameter of m = 0.5. The MAEs for the AC12 test set for different values of the g and m prefactors of these LMF models are plotted in Figure 6 (for raw data see Table S3 in the Supporting Information). The results for the LH-smt-SVWN model (eq 11) are as expected from a previous study of this LMF model for triplet excitation energies in TDDFT.[69] The optimal results are found around m = 0.5 with an MAE of ca. 0.7 kcal/mol with any further increase of the opposite spin-channel contribution (m < 0.5) marginally affecting the MAEs until they increase again for the most extreme choice of m = 0, i.e., $a_\sigma^{smt} = a_\sigma^{ot}$ (eq 12c). The optimal choice for the LMF prefactor g at m = 0.5 is $g \approx 0.7$. Indeed, the LHs that are particularly successful for the AC12 test set, i.e., LH12ct-SsirPW92 (g = 0.646), LH12ct-SsifPW92 (g = 0.709), and LH20t (g = 0.715) are all close to this optimal choice (see above). We also tried to combine the LYP correlation energy functional with smt-LMF based local hybrids to benefit from the error compensation of the LYP correlation functional (see Table S3 in the Supporting Information). However, no improvements over SVWN based LHs were found when the LMF prefactor g and the spin mixing factor m were scanned (following the same procedure as for the plots in Figure 6). This provides further indirect evidence that for certain choices of the LMF, local hybrids are able to overcome any systematic errors in the ST gaps, leaving no room for error compensation from the LYP correlation functional to further improve the results.

https://doi.org/10.1021/acs.jpca.4c02852
J. Phys. Chem. A 2024, 128, 6046−6060

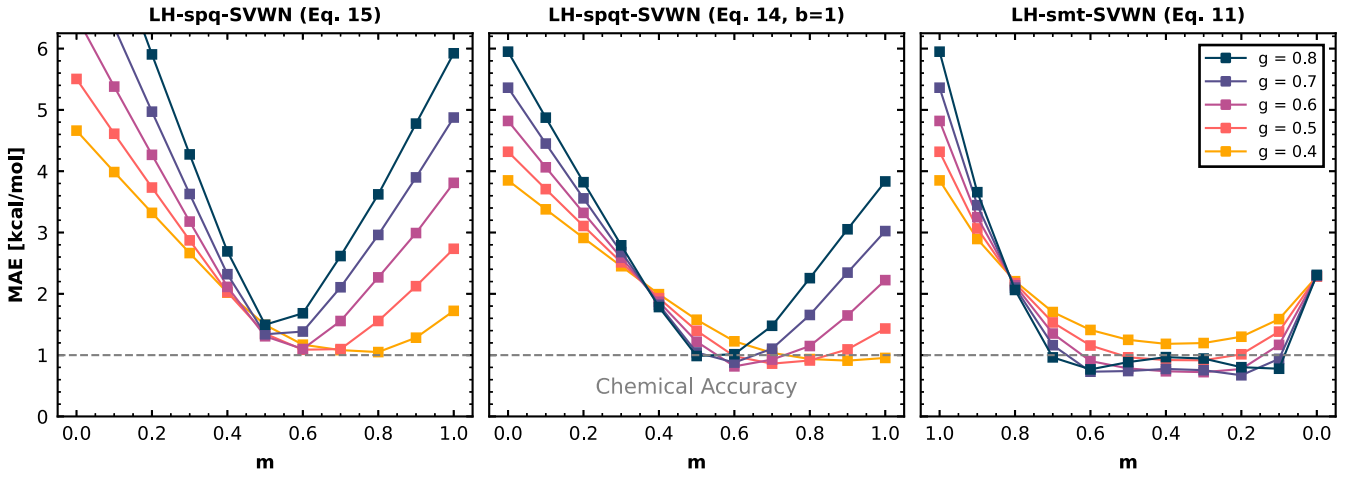

Figure 6. Dependence of the mean absolute error for the AC12 test set on the scaling prefactor g and the spin mixing parameter m in different LMF models. Different scales for m ensure that the contribution of the spin mixing terms increases from left to right within the respective model.

With the spq-LMF (eq 15), the errors for the ST gaps are systematically reduced as m is increased from $m = 0$ (no contribution from the spin polarization term $\zeta(\mathbf{r})$) until a minimum is reached for $m \geq 0.5$, where the optimal value of m depends on the overall prefactor g (Figure 6). For certain choices of m and g, LH-spq-SVWN achieves close to chemical accuracy. This is remarkable because the spq-LMF simplifies to a constant for a singlet state, effectively turning an LH into a GH functional. For the triplet state, the real-space dependence is governed by the spin polarization alone, without the use of the iso-orbital or inhomogeneity indicators. In comparison, for $m = 0$, i.e., using a GH for both the singlet and triplet states, all choices of g lead to much larger errors. However, for some choices of the prefactor g, the MAE for the AC12 test set cannot be reduced significantly below 1.5 kcal/mol by increasing m ($g = 0.8$, blue line in Figure 6).

This limitation is overcome by the spqt-LMF (eq 14, $b = 1$) for which chemical accuracy can be reached for all values $0.4 \leq g \leq 0.8$ by tuning m. Compared to the spq-LMF, the spqt-LMF also uses $t_\sigma(\mathbf{r})$ to detect iso-orbital regions and maintains a real-space dependency for both the singlet state and for choosing $m = 0$.

For more detailed insights in the importance of the iso-orbital indicator $t_\sigma(\mathbf{r})$ for the performance of LHs for ST gaps, the AC12 test set is evaluated scanning the parameter b along with m and g in the spqt-LMF (Figure 7). This three-parameter scan contains some of the results discussed above as the special cases $b = 0$ (Figure 6, left panel) and $b = 1$ (Figure 6, middle panel). Overall, this scan shows that while there is generally a wide range of parameter choices for which the LH-spqt-SVWN functional can achieve chemical accuracy, for $m = 0$, i.e. in the absence of the spin polarization term $\zeta(\mathbf{r})$, no choice of b (iso-orbital indicator prefactor) or g (overall prefactor) can reduce the MAE below that obtained with the nonhybrid SVWN functional (2.38 kcal/mol).

At first sight, Figure 7 conspicuously shows that using the iso-orbital indicator term ($bt_\sigma(\mathbf{r})$ in eq 14) is always preferential over a constant ($(1 - b)$ in eq 14) as larger values of b lead to lower MAEs for all choices of g and m. However, this overlooks that using $bt_\sigma(\mathbf{r})$ vs $(1 - b)$ always lowers the spatially averaged value of the LMF. It is not possible to define this spatial averaging unambitiously, but based on previous analysis using a density weighting scheme, an unscaled t-LMF (i.e., the bare iso-orbital indicator $t_\sigma(\mathbf{r})$) roughly averages to a constant mixing factor of 0.6.[57,119,120] Therefore, more meaningful comparisons for the purpose of assessing the importance of $t_\sigma(\mathbf{r})$ should compare rows across different panels of Figure 7 that roughly lead to the same averaged LMF value. For example, ($g = 1$, $b = 1$) is compared to ($g = 0.6$, $b = 0$) and ($g = 0.5$, $b = 0.5$) is compared to ($g = 0.4$, $b = 0$). In these comparisons, the advantages of using $t_\sigma(\mathbf{r})$ appear much more muted compared to the naive comparison of $b = 0$ and $b > 0$ at a fixed value of g. However, also considering that the global minimum of this three-parameter scan is found at ($g = 0.6$, $m = 0.6$, $b = 1$), the conclusion still holds that using the iso-orbital indicator $t_\sigma(\mathbf{r})$ offers additional advantages in calculations of ST-gaps over using only the spin polarization in the construction of the LMF. Presumably, $t_\sigma(\mathbf{r})$ further directs the effects of the spin-channel mixing to those regions in space where they are most desirable.

Real Space Analysis for Methylene. To test this hypothesis, as well as to link the real space dependence of the LMF to the discussion of the NDC energy contribution above, the differences in the NDC terms $e^{\mathrm{NDC}}(\mathbf{r}) = \sum_\sigma [1 - a_\sigma(\mathbf{r})]\,[e^{\mathrm{sl}}_{\mathrm{x},\sigma}(\mathbf{r}) - e^{\mathrm{ex}}_{\mathrm{x},\sigma}(\mathbf{r})]$ for three LMF pairs are plotted in Figure 8, returning here to the methylene molecule for simplicity. The differences are calculated between LMFs that depend on the spin polarization or common LMF (referred to as "spin-nonadditive", sna, in Figure 8) and the respective spin channel LMF ("spin-additive", sa) for the triplet state. The singlet states are described equally by the sna and sa LMFs, hence their contribution to the difference in the ST gaps drops out anyway. We have also plotted the individual LMFs for the singlet and triplet states (Figure S3) but found those plots more difficult to link to the resulting NDC contributions as this requires multiplication with the $[e^{\mathrm{sl}}_{\mathrm{x},\sigma}(\mathbf{r}) - e^{\mathrm{ex}}_{\mathrm{x},\sigma}(\mathbf{r})]$ term, which itself has a nontrivial real space dependence.

In agreement with Figure 5, the sna LMFs lead to higher NDC energy densities than the respective sa LMFs in most regions along the z axis (defined as shown in the inset of Figure 5). That is, relative to the singlet state, the LHs based on sna LMFs reduce nondynamical correlation (i.e., make the NDC energy more positive) in the triplet state. The real space behavior of the triplet NDC energy density difference of the common t-LMF and spin-channel t-LMF (smt-LMF model) is qualitatively different from that observed for the spq(t)-LMFs.

https://doi.org/10.1021/acs.jpca.4c02852
J. Phys. Chem. A 2024, 128, 6046−6060

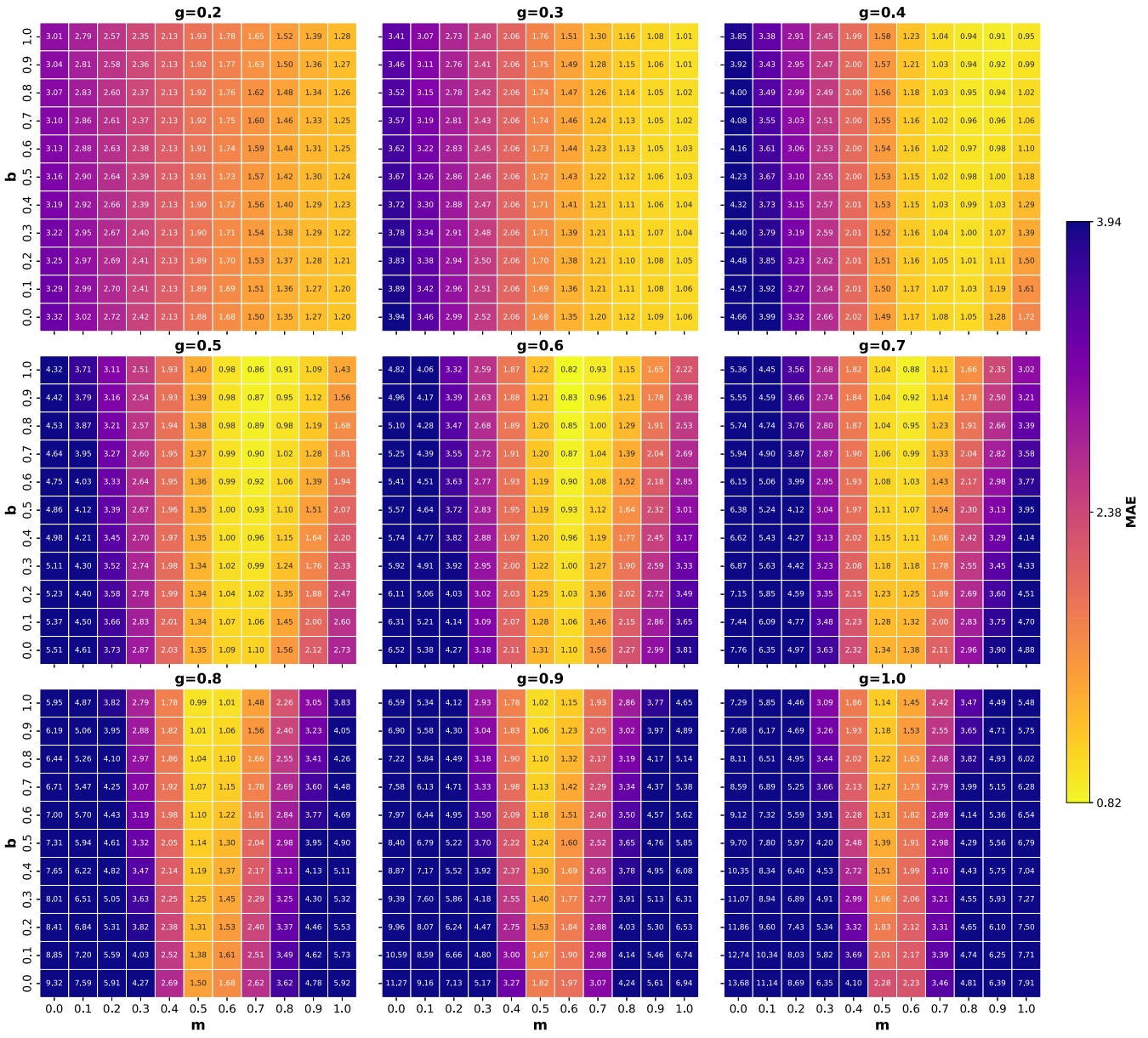

Figure 7. Dependence of the mean absolute error for the AC12 test set on the t-LMF scaling factor b and the spin mixing parameter m in the spqt-LMF (eq 14) using Slater exchange and VWN correlation for the (semi)local energy densities. The color scale is centered at the MAE obtained with pure SVWN (2.38 kcal/mol) and capped at the lowest MAE (0.82 kcal/mol) and 3.94 kcal/mol. The global minimum is found at g = 0.6, b = 1.0, m = 0.6. Note that some of this data is identical to that report in Figure 6 for the spq-LMF (b = 0) and spqt-LMF (b = 1).

It takes the form of two sharp peaks closer to the carbon nucleus whereas the spq(t)-LMF models both lead to broader peaks further away from the nucleus and closer to the spin density maximum. The latter was to be expected as the spq(t)-LMF models explicitly depend on the spin density via the spin polarization $\zeta(\mathbf{r})$. Comparing the spq-LMF and spqt-LMF, it is noted that the use of the iso-orbital indicator in the spqt-LMF helps to avoid the negative triplet NDC energy density difference seen for the spq-LMF, which could explain the slightly superior performance of the spqt-LMF for the ST gaps of the AC12 test set.

Significance for TDDFT. Previous studies of the performance of LHs for triplet states focused on the TDDFT framework to obtain excitation energies. The adiabatic ΔSCF approach chosen in this work has facilitated an in-depth theoretical analysis by taking simple energy differences instead of solving Casida's equations and dealing with potentially nontrivial effects of the XC kernel in TDDFT. Clearly, this has also led to more systematic error compensation. As the new spqt-LMF model was designed for analysis purposes only, we do not aim for a comprehensive assessment of spqt-LMF based LHs for triplet excitation energies in TDDFT. The results for a parameter scan of the spqt-LMF for a subset of the QUEST-ST test set[69,107] of vertical singlet and triplet excitation energies (Figure S6–S8) show overall similar trends as seen for the AC12 test set studied with the adiabatic ΔSCF approach (Figure 7). The most significant difference is that the optimal value of m for triplet states in TDDFT is found at its maximum allowed value of m = 1.0 (compared to m = 0.6 for the AC12 test set).

https://doi.org/10.1021/acs.jpca.4c02852
J. Phys. Chem. A 2024, 128, 6046−6060

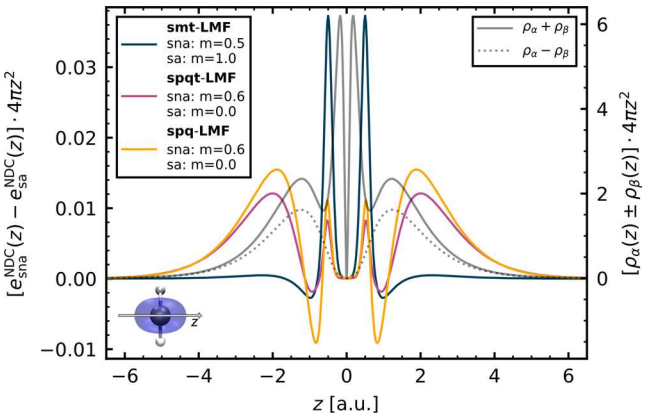

Figure 8. Difference in the triplet state NDC terms $e^{NDC}(\mathbf{r}) = \sum_\sigma [1 - a_\sigma(\mathbf{r})] [e^{sl}_{x,\sigma}(\mathbf{r}) - e^{ex}_{x,\sigma}(\mathbf{r})]$ for a spin-nonadditive (sna) LMF (smt-LMF, m = 0.5, g = 0.709, i.e. common t-LMF; spqt-LMF, b = 1.0, m = 0.6, g = 0.6; spq-LMF, m = 0.6, g = 0.6) and spin-additive (sa) LMF (smt-LMF, m = 1.0, g = 0.709, i.e. spin-channel t-LMF; spqt-LMF, b = 1.0, m = 0.0, g = 0.6; spq-LMF, m = 0.0, g = 0.6) plotted as radial distributions along the p_z-type orbital in the methylene molecule in its triplet ground state. Calculations were performed self-consistently using Slater exchange, VWN correlation, and cc-pV6Z basis sets. The inset shows an iso-surface plot of the spin density and the solid (dotted) gray line is the radial total (spin) density. Note that the interpretation of m for the smt-LMF is different from the spq(t)-LMFs (see main text and caption of Figure 6).

DISCUSSION AND CONCLUSIONS

While the good performance of local hybrids using the common t-LMF for TDDFT triplet excitation energies has been known for some time, their performance for ST gaps for arylcarbenes within UKS/RKS DFT is also remarkable. The ability to predict these energy differences with chemical accuracy without the need for expensive wave function methods or double hybrids extends the reliability and scope of theoretical predictions in practical applications. Despite the technical discussion of the details of the LMF included in this work, DFT calculations with local hybrids in TURBOMOLE are as easy for the user to perform as with any other density functional approximation by specifying a single functional keyword. The seminumerical implementation of local hybrids, together with integral prescreening makes them very efficient tools with a computational cost comparable to that of global hybrids when using standard grid sizes (with a larger prefactor for the gradients).[54,55,121] This work also emphasizes that not all local hybrid functionals achieve outstanding performance for ST gaps with many early local hybrids based on LMFs without spin-channel mixing and the recent first-principle local hybrid TMHF lacking the advantages demonstrated for the common t-LMF based LHs, giving only average performance.

To rationalize the observed trends in ST gaps, we conceive a qualitative scheme of the relevant energy levels in Figure 9. HFKS energies are well-known to greatly underestimate ST gaps because the correlation energy of the singlet state is significantly larger than that of the triplet state. Adding dynamical correlation is insufficient for accurate ST gaps, because a significant portion of the extra correlation present in the singlet state is nondynamical. Semilocal density functional approximations (and, proportionally, their global hybrid versions) can recover a significant fraction of the exact nondynamical correlation of the singlet state, but they (relatively) overestimate it for the triplet state, because the

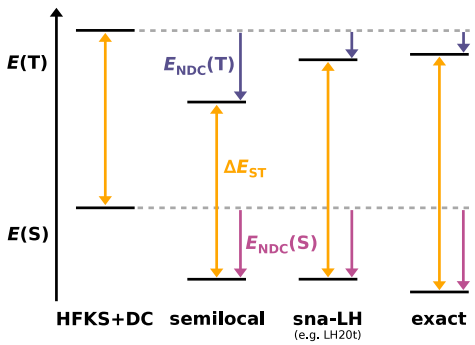

Figure 9. Schematic diagram of the singlet and triplet energy levels and the magnitude of the nondynamical correlation energy (NDC) with different models compared to the energy expectation value of the KS determinant plus dynamical correlation (HFKS+DC) and the exact solution. The overstabilization of the triplet state by NDC with semilocal functionals (or similarly, GHs and sa-LHs) is reduced with sna-LHs (common t-LMF or spqt-LMF based LHs) increasing the ST gap. The energy axis is not to scale and differences are stylized for clarity.

difference between semilocal and exact exchange exhibits exchange-like spin scaling. Spin-nonadditive local hybrids such as common t-LMF or spqt-LMF based LHs address this shortcoming by scaling down nondynamical correlation in the triplet state. The spin-nonadditivity implies that E^{LH}_{NDC} cannot be understood as "hybrid exchange", but should indeed be considered (and constructed as) a model of nondynamical correlation.

Our empirical studies of model LMFs suggest that although a large part of this effect can be explained by the spin mixing scheme used, chemical accuracy is not reached with simpler LMFs whose real space dependence is solely controlled by the spin polarization. Only when the iso-orbital indicator was included in explicitly spin polarization dependent LMFs to further reduce self-interaction, the triplet state nondynamical correlation energy decreases to an extent comparable to that seen the common t-LMF, leading to chemically accurate predictions of the ST gaps for arylcarbenes. Overall, the common t-LMF model (or its smt-LMF generalization) remains preferable because excellent performance for ST gaps is achieved for a much wider range of values of the two parameters m and g, leaving ample room for future theoretical or empirical constraints.

ASSOCIATED CONTENT

Supporting Information

The Supporting Information is available free of charge at https://pubs.acs.org/doi/10.1021/acs.jpca.4c02852.

Individual excitation energies (eV) of the QUEST-ST subset for the scan of the parameters b, m, and g in the spqt-LMF based LHs (CSV)

Explanations, tables and figures with additional computational data, and raw data (PDF)

AUTHOR INFORMATION

Corresponding Authors

Robin Grotjahn − *Department of Chemistry, University of California, Irvine, Irvine, California 92697-2025, United States;* orcid.org/0000-0002-7160-2581; Email: robin.grotjahn@uci.edu

https://doi.org/10.1021/acs.jpca.4c02852
J. Phys. Chem. A 2024, 128, 6046−6060

Filipp Furche − *Department of Chemistry, University of California, Irvine, Irvine, California 92697-2025, United States;* orcid.org/0000-0001-8520-3971; Email: filipp.furche@uci.edu

Authors

Justin Purnomo − *Department of Chemistry, University of California, Irvine, Irvine, California 92697-2025, United States;* Present Address: Department of Chemistry and Biochemistry, University of California, Los Angeles, California 90095, United States. (J.P.)

Dayun Jin − *Department of Chemistry, University of California, Irvine, Irvine, California 92697-2025, United States;* orcid.org/0009-0008-1525-9505

Nicolas Lutfi − *Department of Chemistry, University of California, Irvine, Irvine, California 92697-2025, United States;* orcid.org/0009-0001-4293-8393

Complete contact information is available at: https://pubs.acs.org/10.1021/acs.jpca.4c02852

Author Contributions

R. Grotjahn: Conceptualization (lead), Methodology (lead), Software (lead), Validation (equal), Formal analysis (lead), Investigation (lead), Data Curation (equal), Writing - Original Draft (lead), Writing - Review & Editing (equal), Visualization (equal), Supervision (equal), Project administration (equal), Funding acquisition (equal); **J. Purnomo**: Methodology (supporting), Validation (equal), Formal analysis (supporting), Investigation (supporting), Data Curation (supporting), Writing - Original Draft (supporting), Writing - Review & Editing (supporting), Visualization (equal), Funding acquisition (supporting); **D. Jin**: Software (supporting), Formal analysis (supporting), Investigation (supporting), Writing - Review & Editing (supporting); **N. Lutfi**: Software (supporting), Investigation (supporting), Data Curation (supporting), Writing - Original Draft (supporting), Writing - Review & Editing (supporting), Visualization (supporting); **F. Furche**: Conceptualization (supporting), Methodology (supporting), Software (supporting), Validation (supporting), Formal analysis (supporting), Data Curation (supporting), Writing - Original Draft (supporting), Writing - Review & Editing (equal), Visualization (supporting), Supervision (equal), Project administration (equal), Funding acquisition (equal).

Notes

The authors declare the following competing financial interest(s): Principal Investigator Filipp Furche has an equity interest in TURBOMOLE GmbH. The terms of this arrangement have been reviewed and approved by the University of California, Irvine, in accordance with its conflict of interest policies.

■ ACKNOWLEDGMENTS

R. G. acknowledges support via a Walter-Benjamin postdoctoral fellowship funded by the Deutsche Forschungsgemeinschaft (DFG, German Research Foundation) − 501114520. J. P. acknowledges support via an undergraduate research fellowship funded by the University of California Leadership Excellence through Advanced Degrees (UC LEADS) program. This material is based upon work supported by the National Science Foundation under Grant No. CHE-2102568. This work utilized the infrastructure for high-performance and high-throughput computing, research data storage and analysis, and scientific software tool integration built, operated, and updated by the Research Cyberinfrastructure Center (RCIC) at the University of California, Irvine (UCI).

■ REFERENCES

(1) Sheridan, R. S. Heteroarylcarbenes. *Chem. Rev.* **2013**, *113*, 7179−7208.
(2) Peris, E. Smart N-Heterocyclic Carbene Ligands in Catalysis. *Chem. Rev.* **2018**, *118*, 9988−10031.
(3) Kuwata, S.; Hahn, F. E. Complexes Bearing Protic N-Heterocyclic Carbene Ligands. *Chem. Rev.* **2018**, *118*, 9642−9677.
(4) Huynh, H. V. Electronic Properties of N-Heterocyclic Carbenes and Their Experimental Determination. *Chem. Rev.* **2018**, *118*, 9457−9492.
(5) Cheng, J.; Wang, L.; Wang, P.; Deng, L. High-Oxidation-State 3d Metal (Ti−Cu) Complexes with *N*-Heterocyclic Carbene Ligation. *Chem. Rev.* **2018**, *118*, 9930−9987.
(6) Vivancos, Á.; Segarra, C.; Albrecht, M. Mesoionic and Related Less Heteroatom-Stabilized N-Heterocyclic Carbene Complexes: Synthesis, Catalysis, and Other Applications. *Chem. Rev.* **2018**, *118*, 9493−9586.
(7) Nesterov, V.; Reiter, D.; Bag, P.; Frisch, P.; Holzner, R.; Porzelt, A.; Inoue, S. NHCs in Main Group Chemistry. *Chem. Rev.* **2018**, *118*, 9678−9842.
(8) Nemirowski, A.; Schreiner, P. R. Electronic Stabilization of Ground State Triplet Carbenes. *J. Org. Chem.* **2007**, *72*, 9533−9540.
(9) Hirai, K.; Itoh, T.; Tomioka, H. Persistent Triplet Carbenes. *Chem. Rev.* **2009**, *109*, 3275−3332.
(10) Henkel, S.; Costa, P.; Klute, L.; Sokkar, P.; Fernandez-Oliva, M.; Thiel, W.; Sanchez-Garcia, E.; Sander, W. Switching the Spin State of Diphenylcarbene via Halogen Bonding. *J. Am. Chem. Soc.* **2016**, *138*, 1689−1697.
(11) Woodworth, R. C.; Skell, P. S. Methylene, CH_2. Stereospecific Reaction with cis- and trans-2-Butene. *J. Am. Chem. Soc.* **1959**, *81*, 3383−3386.
(12) Harrison, J. F.; Allen, L. C. Electronic structure of methylene. *J. Am. Chem. Soc.* **1969**, *91*, 807−823.
(13) O'Neil, S. V.; Schaefer, H. F.; Bender, C. F. C_{2v} Potential Energy Surfaces for Seven Low-Lying States of CH_2. *J. Chem. Phys.* **1971**, *55*, 162−169.
(14) Sander, W.; Hübert, R.; Kraka, E.; Gräfenstein, J.; Cremer, D. 4-Oxo-2,3,5,6-tetrafluorocyclohexa-2,5-dienylidene—A Highly Electrophilic Triplet Carbene. *Chem. Eur. J.* **2000**, *6*, 4567−4579.
(15) Pause, L.; Robert, M.; Heinicke, J.; Kühl, O. Radical anions of carbenes and carbene homologues. DFT study and preliminary experimental results. *J. Chem. Soc., Perkin trans. II* **2001**, 1383−1388.
(16) Wang, X.; Agarwal, J.; Schaefer III, H. F. Characterizing a nonclassical carbene with coupled cluster methods: cyclobutylidene. *Phys. Chem. Chem. Phys.* **2016**, *18*, 24560−24568.
(17) Song, X.-F.; Li, Z.-W.; Chen, W.-K.; Gao, Y.-J.; Cui, G. Thermally Activated Delayed Fluorescence Mechanism of a Bicyclic "Carbene−Metal−Amide" Copper Compound: DFT/MRCI Studies and Roles of Excited-State Structure Relaxation. *Inorg. Chem.* **2022**, *61*, 7673−7681.
(18) Riplinger, C.; Neese, F. An efficient and near linear scaling pair natural orbital based local coupled cluster method. *J. Chem. Phys.* **2013**, *138*, 034106.
(19) Riplinger, C.; Sandhoefer, B.; Hansen, A.; Neese, F. Natural triple excitations in local coupled cluster calculations with pair natural orbitals. *J. Chem. Phys.* **2013**, *139*, 134101.
(20) Liakos, D. G.; Sparta, M.; Kesharwani, M. K.; Martin, J. M. L.; Neese, F. Exploring the Accuracy Limits of Local Pair Natural Orbital Coupled-Cluster Theory. *J. Chem. Theory Comput.* **2015**, *11*, 1525−1539.
(21) Saitow, M.; Becker, U.; Riplinger, C.; Valeev, E. F.; Neese, F. A new near-linear scaling, efficient and accurate, open-shell domain-based local pair natural orbital coupled cluster singles and doubles theory. *J. Chem. Phys.* **2017**, *146*, 164105.

(22) Ho, L. P.; Nasr, A.; Jones, P. G.; Altun, A.; Neese, F.; Bistoni, G.; Tamm, M. London Dispersion Interactions in Pnictogen Cations $[ECl]_2^+$ and $[E = E]^{2+}$ (E = P, As, Sb) Supported by Anionic *N*-Heterocyclic Carbenes. *Chem. Eur. J.* **2018**, *24*, 18922−18932.
(23) Ghafarian Shirazi, R.; Neese, F.; Pantazis, D. A.; Bistoni, G. Physical Nature of Differential Spin-State Stabilization of Carbenes by Hydrogen and Halogen Bonding: A Domain-Based Pair Natural Orbital Coupled Cluster Study. *J. Phys. Chem. A* **2019**, *123*, 5081−5090.
(24) Ghafarian Shirazi, R.; Neese, F.; Pantazis, D. A. Accurate Spin-State Energetics for Aryl Carbenes. *J. Chem. Theory Comput.* **2018**, *14*, 4733−4746.
(25) Shirazi, R. G.; Pantazis, D. A.; Neese, F. Performance of density functional theory and orbital-optimised second-order perturbation theory methods for geometries and singlet−triplet state splittings of aryl-carbenes. *Mol. Phys.* **2020**, *118*, e1764644.
(26) Grimme, S. Semiempirical hybrid density functional with perturbative second-order correlation. *J. Chem. Phys.* **2006**, *124*, 034108.
(27) Goerigk, L.; Grimme, S. Efficient and Accurate Double-Hybrid-Meta-GGA Density Functionals—Evaluation with the Extended GMTKN30 Database for General Main Group Thermochemistry, Kinetics, and Noncovalent Interactions. *J. Chem. Theory Comput.* **2011**, *7*, 291−309.
(28) Becke, A. D. Density-functional thermochemistry. III. *The role of exact exchange. J. Chem. Phys.* **1993**, *98*, 5648−5652.
(29) Lee, C.; Yang, W.; Parr, R. G. Development of the Colle-Salvetti correlation-energy formula into a functional of the electron density. *Phys. Rev. B* **1988**, *37*, 785−789.
(30) Stephens, P. J.; Devlin, F. J.; Chabalowski, C. F.; Frisch, M. J. Ab Initio Calculation of Vibrational Absorption and Circular Dichroism Spectra Using Density Functional Force Fields. *J. Phys. Chem.* **1994**, *98*, 11623−11627.
(31) Staroverov, V. N.; Scuseria, G. E.; Tao, J.; Perdew, J. P. Comparative assessment of a new nonempirical density functional: Molecules and hydrogen-bonded complexes. *J. Chem. Phys.* **2003**, *119*, 12129−12137.
(32) Adamo, C.; Barone, V. Exchange functionals with improved long-range behavior and adiabatic connection methods without adjustable parameters: The mPW and mPW1PW models. *J. Chem. Phys.* **1998**, *108*, 664−675.
(33) Schwabe, T.; Grimme, S. Towards chemical accuracy for the thermodynamics of large molecules: new hybrid density functionals including non-local correlation effects. *Phys. Chem. Chem. Phys.* **2006**, *8*, 4398.
(34) Chai, J.-D.; Head-Gordon, M. Systematic optimization of long-range corrected hybrid density functionals. *J. Chem. Phys.* **2008**, *128*, 084106.
(35) Lin, Y.-S.; Li, G.-D.; Mao, S.-P.; Chai, J.-D. Long-Range Corrected Hybrid Density Functionals with Improved Dispersion Corrections. *J. Chem. Theory Comput.* **2013**, *9*, 263−272.
(36) Zhao, Y.; Truhlar, D. G. The M06 suite of density functionals for main group thermochemistry, thermochemical kinetics, noncovalent interactions, excited states, and transition elements: two new functionals and systematic testing of four M06-class functionals and 12 other functionals. *Theor. Chem. Acc.* **2008**, *120*, 215−241.
(37) Jaramillo, J.; Scuseria, G. E.; Ernzerhof, M. Local hybrid functionals. *J. Chem. Phys.* **2003**, *118*, 1068−1073.
(38) Maier, T. M.; Arbuznikov, A. V.; Kaupp, M. Local hybrid functionals: Theory, implementation, and performance of an emerging new tool in quantum chemistry and beyond. *Rev. Comput. Mol. Sci.* **2019**, *9*, e1378.
(39) Janesko, B. G. Replacing hybrid density functional theory: motivation and recent advances. *Chem. Soc. Rev.* **2021**, *50*, 8470−8495.
(40) Bahmann, H. From global to local − hybrid density functionals for weak and strong correlation. *Chemical Modelling* **2021**, *16*, 165−181.
(41) Henderson, T. M.; Scuseria, G. E. The connection between self-interaction and static correlation: a random phase approximation perspective. *Mol. Phys.* **2010**, *108*, 2511−2517.
(42) Arbuznikov, A. V.; Kaupp, M. Local hybrid exchange-correlation functionals based on the dimensionless density gradient. *Chem. Phys. Lett.* **2007**, *440*, 160−168.
(43) Bahmann, H.; Rodenberg, A.; Arbuznikov, A. V.; Kaupp, M. A thermochemically competitive local hybrid functional without gradient corrections. *J. Chem. Phys.* **2007**, *126*, 011103.
(44) Kaupp, M.; Bahmann, H.; Arbuznikov, A. V. Local hybrid functionals: An assessment for thermochemical kinetics. *J. Chem. Phys.* **2007**, *127*, 194102.
(45) Haasler, M.; Maier, T. M.; Grotjahn, R.; Gückel, S.; Arbuznikov, A. V.; Kaupp, M. A Local Hybrid Functional with Wide Applicability and Good Balance between (De)Localization and Left−Right Correlation. *J. Chem. Theory Comput.* **2020**, *16*, 5645−5657.
(46) Grotjahn, R.; Kaupp, M. A Look at Real-World Transition-Metal Thermochemistry and Kinetics with Local Hybrid Functionals. *Isr. J. Chem.* **2023**, *63*, e202200021.
(47) Fürst, S.; Haasler, M.; Grotjahn, R.; Kaupp, M. Full Implementation, Optimization, and Evaluation of a Range-Separated Local Hybrid Functional with Wide Accuracy for Ground and Excited States. *J. Chem. Theory Comput.* **2023**, *19*, 488−502.
(48) Haasler, M.; Maier, T. M.; Kaupp, M. Toward a correct treatment of core properties with local hybrid functionals. *J. Comput. Chem.* **2023**, *44*, 2461−2477.
(49) Plessow, P.; Weigend, F. Seminumerical calculation of the Hartree-Fock exchange matrix: Application to two-component procedures and efficient evaluation of local hybrid density functionals. *J. Comput. Chem.* **2012**, *33*, 810−816.
(50) Laqua, H.; Kussmann, J.; Ochsenfeld, C. Efficient and Linear-Scaling Seminumerical Method for Local Hybrid Density Functionals. *J. Chem. Theory Comput.* **2018**, *14*, 3451−3458.
(51) Laqua, H.; Thompson, T. H.; Kussmann, J.; Ochsenfeld, C. Highly Efficient, Linear-Scaling Seminumerical Exact-Exchange Method for Graphic Processing Units. *J. Chem. Theory Comput.* **2020**, *16*, 1456−1468.
(52) Balasubramani, S. G.; Chen, G. P.; Coriani, S.; Diedenhofen, M.; Frank, M. S.; Franzke, Y. J.; Furche, F.; Grotjahn, R.; Harding, M. E.; Hättig, C.; et al. TURBOMOLE: Modular program suite for ab initio quantum-chemical and condensed-matter simulations. *J. Chem. Phys.* **2020**, *152*, 184107.
(53) Franzke, Y. J.; Holzer, C.; Andersen, J. H.; Begušić, T.; Bruder, F.; Coriani, S.; Della Sala, F.; Fabiano, E.; Fedotov, D. A.; Fürst, S.; et al. TURBOMOLE: Today and Tomorrow. *J. Chem. Theory Comput.* **2023**, *19*, 6859−6890.
(54) Bahmann, H.; Kaupp, M. Efficient Self-Consistent Implementation of Local Hybrid Functionals. *J. Chem. Theory Comput.* **2015**, *11*, 1540−1548.
(55) Klawohn, S.; Bahmann, H.; Kaupp, M. Implementation of Molecular Gradients for Local Hybrid Density Functionals Using Seminumerical Integration Techniques. *J. Chem. Theory Comput.* **2016**, *12*, 4254−4262.
(56) Maier, T. M.; Bahmann, H.; Kaupp, M. Efficient Seminumerical Implementation of Global and Local Hybrid Functionals for Time-Dependent Density Functional Theory. *J. Chem. Theory Comput.* **2015**, *11*, 4226−4237.
(57) Grotjahn, R.; Furche, F.; Kaupp, M. Development and Implementation of Excited-State Gradients for Local Hybrid Functionals. *J. Chem. Theory Comput.* **2019**, *15*, 5508−5522.
(58) Grotjahn, R.; Lauter, G. J.; Haasler, M.; Kaupp, M. Evaluation of Local Hybrid Functionals for Electric Properties: Dipole Moments and Static and Dynamic Polarizabilities. *J. Phys. Chem. A* **2020**, *124*, 8346−8358.
(59) Kehry, M.; Franzke, Y. J.; Holzer, C.; Klopper, W. Quasirelativistic two-component core excitations and polarisabilities from a damped-response formulation of the Bethe−Salpeter equation. *Mol. Phys.* **2020**, *118*, e1755064.

https://doi.org/10.1021/acs.jpca.4c02852
J. Phys. Chem. A 2024, 128, 6046−6060

(60) Holzer, C.; Franzke, Y. J.; Kehry, M. Assessing the Accuracy of Local Hybrid Density Functional Approximations for Molecular Response Properties. *J. Chem. Theory Comput.* **2021**, *17*, 2928−2947.
(61) Haunschild, R.; Scuseria, G. E. Range-separated local hybrids. *J. Chem. Phys.* **2010**, *132*, 224106.
(62) Fürst, S.; Kaupp, M. Accurate Ionization Potentials, Electron Affinities, and Band Gaps from the ωLH22t Range-Separated Local Hybrid Functional: No Tuning Required. *J. Chem. Theory Comput.* **2023**, *19*, 3146−3158.
(63) Grotjahn, R. Learning from the 4-(dimethylamino)benzonitrile twist: Two-parameter range-separated local hybrid functional with high accuracy for triplet and charge-transfer excitations. *J. Chem. Phys.* **2023**, *159*, 174102.
(64) Grotjahn, R.; Maier, T. M.; Michl, J.; Kaupp, M. Development of a TDDFT-Based Protocol with Local Hybrid Functionals for the Screening of Potential Singlet Fission Chromophores. *J. Chem. Theory Comput.* **2017**, *13*, 4984−4996.
(65) Grotjahn, R.; Kaupp, M. Validation of Local Hybrid Functionals for Excited States: Structures, Fluorescence, Phosphorescence, and Vibronic Spectra. *J. Chem. Theory Comput.* **2020**, *16*, 5821−5834.
(66) Wen, J.; Turowski, M.; Dron, P. I.; Chalupský, J.; Grotjahn, R.; Maier, T. M.; Fatur, S. M.; Havlas, Z.; Johnson, J. C.; Kaupp, M.; et al. Electronic States of 2,3-Diamino-1,4-naphthoquinone and Its N-Alkylated Derivatives. *J. Phys. Chem. C* **2020**, *124*, 60−69.
(67) Maier, T. M.; Bahmann, H.; Arbuznikov, A. V.; Kaupp, M. Validation of local hybrid functionals for TDDFT calculations of electronic excitation energies. *J. Chem. Phys.* **2016**, *144*, 074106.
(68) Grotjahn, R.; Kaupp, M. Reliable TDDFT Protocol Based on a Local Hybrid Functional for the Prediction of Vibronic Phosphorescence Spectra Applied to Tris(2,2′-bipyridine)-Metal Complexes. *J. Phys. Chem. A* **2021**, *125*, 7099−7110.
(69) Grotjahn, R.; Kaupp, M. Assessment of hybrid functionals for singlet and triplet excitations: Why do some local hybrid functionals perform so well for triplet excitation energies? *J. Chem. Phys.* **2021**, *155*, 124108.
(70) Arbuznikov, A. V.; Kaupp, M. Importance of the correlation contribution for local hybrid functionals: Range separation and self-interaction corrections. *J. Chem. Phys.* **2012**, *136*, 014111.
(71) Becke, A. D. A new inhomogeneity parameter in density-functional theory. *J. Chem. Phys.* **1998**, *109*, 2092−2098.
(72) Oliver, G. L.; Perdew, J. P. Spin-density gradient expansion for the kinetic energy. *Phys. Rev. A* **1979**, *20*, 397−403.
(73) Tao, J.; Perdew, J. P.; Staroverov, V. N.; Scuseria, G. E. Climbing the Density Functional Ladder: Nonempirical Meta−Generalized Gradient Approximation Designed for Molecules and Solids. *Phys. Rev. Lett.* **2003**, *91*, 146401.
(74) Arbuznikov, A. V.; Bahmann, H.; Kaupp, M. Local Hybrid Functionals with an Explicit Dependence on Spin Polarization. *J. Phys. Chem. A* **2009**, *113*, 11898−11906.
(75) Perdew, J. P.; Staroverov, V. N.; Tao, J.; Scuseria, G. E. Density functional with full exact exchange, balanced nonlocality of correlation, and constraint satisfaction. *Phys. Rev. A* **2008**, *78*, 052513.
(76) Schmidt, T.; Kraisler, E.; Makmal, A.; Kronik, L.; Kümmel, S. A self-interaction-free local hybrid functional: Accurate binding energies vis-à-vis accurate ionization potentials from Kohn-Sham eigenvalues. *J. Chem. Phys.* **2014**, *140*, 18A510.
(77) Maier, T. M. Locally Range-Separated Local Hybrid Functionals − The Next Level on the Hybrid Functional Ladder. 2023; *ChemRxiv*, submitted 2023−03−27, DOI: 10.26434/chemrxiv-2023-5m7jb, accessed 2024−06−12.
(78) Fürst, S.; Kaupp, M.; Wodyński, A. Range-Separated Local Hybrid Functionals with Small Fractional-Charge and Fractional-Spin Errors: Escaping the Zero-Sum Game of DFT Functionals. *J. Chem. Theory Comput.* **2023**, *19*, 8639−8653.
(79) TURBOMOLE V7.8 2023, a development of University of Karlsruhe and Forschungszentrum Karlsruhe GmbH, 1989−2007, TURBOMOLE GmbH, since 2007; available from https://www.turbomole.org, accessed 2024−06−12.
(80) Arbuznikov, A. V.; Kaupp, M. Towards improved local hybrid functionals by calibration of exchange-energy densities. *J. Chem. Phys.* **2014**, *141*, 204101.
(81) Holzer, C.; Franzke, Y. J. A local hybrid exchange functional approximation from first principles. *J. Chem. Phys.* **2022**, *157*, 034108.
(82) Perdew, J. P.; Burke, K.; Ernzerhof, M. Generalized gradient approximation made simple. *Phys. Rev. Lett.* **1996**, *77*, 3865−3868.
(83) Becke, A. D. Density-functional exchange-energy approximation with correct asymptotic behavior. *Phys. Rev. A* **1988**, *38*, 3098−3100.
(84) Sun, J.; Ruzsinszky, A.; Perdew, J. P. Strongly Constrained and Appropriately Normed Semilocal Density Functional. *Phys. Rev. Lett.* **2015**, *115*, 036402.
(85) Furness, J. W.; Kaplan, A. D.; Ning, J.; Perdew, J. P.; Sun, J. Accurate and Numerically Efficient r^2SCAN Meta-Generalized Gradient Approximation. *J. Phys. Chem. Lett.* **2020**, *11*, 8208−8215.
(86) Zhao, Y.; Truhlar, D. G. A new local density functional for main-group thermochemistry, transition metal bonding, thermochemical kinetics, and noncovalent interactions. *J. Chem. Phys.* **2006**, *125*, 194101.
(87) Adamo, C.; Barone, V. Toward reliable density functional methods without adjustable parameters: The PBE0 model. *J. Chem. Phys.* **1999**, *110*, 6158−6170.
(88) Hui, K.; Chai, J.-D. SCAN-based hybrid and double-hybrid density functionals from models without fitted parameters. *J. Chem. Phys.* **2016**, *144*, 044114.
(89) Yanai, T.; Tew, D. P.; Handy, N. C. A new hybrid exchange−correlation functional using the Coulomb-attenuating method (CAM-B3LYP). *Chem. Phys. Lett.* **2004**, *393*, 51−57.
(90) Mardirossian, N.; Head-Gordon, M. ωB97M-V: A combinatorially optimized, range-separated hybrid, meta-GGA density functional with VV10 nonlocal correlation. *J. Chem. Phys.* **2016**, *144*, 214110.
(91) Grimme, S.; Antony, J.; Ehrlich, S.; Krieg, H. A consistent and accurate ab initioparametrization of density functional dispersion correction (DFT-D) for the 94 elements H-Pu. *J. Chem. Phys.* **2010**, *132*, 154104.
(92) Becke, A. D.; Johnson, E. R. A density-functional model of the dispersion interaction. *J. Chem. Phys.* **2005**, *123*, 154101.
(93) Caldeweyher, E.; Bannwarth, C.; Grimme, S. Extension of the D3 dispersion coefficient model. *J. Chem. Phys.* **2017**, *147*, 034112.
(94) Caldeweyher, E.; Ehlert, S.; Hansen, A.; Neugebauer, H.; Spicher, S.; Bannwarth, C.; Grimme, S. A generally applicable atomic-charge dependent London dispersion correction. *J. Chem. Phys.* **2019**, *150*, 154122.
(95) Caldeweyher, E.; Mewes, J.-M.; Ehlert, S.; Grimme, S. Extension and evaluation of the D4 London-dispersion model for periodic systems. *Phys. Chem. Chem. Phys.* **2020**, *22*, 8499−8512.
(96) Perdew, J. P.; Savin, A.; Burke, K. Escaping the symmetry dilemma through a pair-density interpretation of spin-density functional theory. *Phys. Rev. A* **1995**, *51*, 4531−4541.
(97) Gräfenstein, J.; Kraka, E.; Cremer, D. Density functional theory for open-shell singlet biradicals. *Chem. Phys. Lett.* **1998**, *288*, 593−602.
(98) Gräfenstein, J.; Kraka, E.; Filatov, M.; Cremer, D. Can Unrestricted Density-Functional Theory Describe Open Shell Singlet Biradicals? *Int. J. Mol. Sci.* **2002**, *3*, 360−394.
(99) Dunning, T. H., Jr. Gaussian basis sets for use in correlated molecular calculations. I. The atoms boron through neon and hydrogen. *J. Chem. Phys.* **1989**, *90*, 1007−1023.
(100) Peterson, K. A.; Woon, D. E.; Dunning, T. H. Benchmark calculations with correlated molecular wave functions. IV. The classical barrier height of the H + H_2→H_2+H reaction. *J. Chem. Phys.* **1994**, *100*, 7410−7415.
(101) Wilson, A. K.; van Mourik, T.; Dunning, T. H. Gaussian basis sets for use in correlated molecular calculations. VI. Sextuple zeta correlation consistent basis sets for boron through neon. *J. Mol. Struc-THEOCHEM* **1996**, *388*, 339−349.

(102) Weigend, F.; Furche, F.; Ahlrichs, R. Gaussian basis sets of quadruple zeta valence quality for atoms H−Kr. *J. Chem. Phys.* **2003**, *119*, 12753−12762.
(103) Rappoport, D.; Furche, F. Property-optimized Gaussian basis sets for molecular response calculations. *J. Chem. Phys.* **2010**, *133*, 134105.
(104) Weigend, F.; Ahlrichs, R. Balanced basis sets of split valence, triple zeta valence and quadruple zeta valence quality for H to Rn: Design and assessment of accuracy. *Phys. Chem. Chem. Phys.* **2005**, *7*, 3297−3305.
(105) Eichkorn, K.; Treutler, O.; Öhm, H.; Häser, M.; Ahlrichs, R. Auxiliary basis sets to approximate Coulomb potentials. *Chem. Phys. Lett.* **1995**, *240*, 283−290.
(106) Weigend, F. Accurate Coulomb-fitting basis sets for H to Rn. *Phys. Chem. Chem. Phys.* **2006**, *8*, 1057−1065.
(107) Véril, M.; Scemama, A.; Caffarel, M.; Lipparini, F.; Boggio-Pasqua, M.; Jacquemin, D.; Loos, P.-F. QUESTDB: A database of highly accurate excitation energies for the electronic structure community. *Wiley Interdiscip. Rev. Comput. Mol. Sci.* **2021**, *11*, e1517.
(108) Kendall, R. A.; Dunning, T. H.; Harrison, R. J. Electron affinities of the first-row atoms revisited. Systematic basis sets and wave functions. *J. Chem. Phys.* **1992**, *96*, 6796−6806.
(109) Petek, H.; Nesbitt, D. J.; Darwin, D. C.; Ogilby, P. R.; Moore, C. B.; Ramsay, D. A. Analysis of CH_2 $\tilde{a}$ $^1A_1$ (1,0,0) and (0,0,1) Coriolis-coupled states, $\tilde{a}$ $^1A_1$−$\tilde{X}$ $^3B_1$ spin-orbit coupling, and the equilibrium structure of CH_2 $\tilde{a}$ $^1A_1$ state. *J. Chem. Phys.* **1989**, *91*, 6566−6578.
(110) Jensen, P.; Bunker, P. R. The potential surface and stretching frequencies of $\tilde{X}$ $^3B_1$ methylene (CH_2) determined from experiment using the Morse oscillator-rigid bender internal dynamics Hamiltonian. *J. Chem. Phys.* **1988**, *89*, 1327−1332.
(111) Huron, B.; Malrieu, J. P.; Rancurel, P. Iterative perturbation calculations of ground and excited state energies from multiconfigurational zeroth-order wavefunctions. *J. Chem. Phys.* **1973**, *58*, 5745−5759.
(112) Neese, F. Software update: the ORCA program system, version 4.0. Wiley Interdiscip. *Rev. Comput. Mol. Sci.* **2018**, *8*, e1327.
(113) Peach, M. J. G.; Williamson, M. J.; Tozer, D. J. Influence of Triplet Instabilities in TDDFT. J. *Chem. Theory Comput.* **2011**, *7*, 3578−3585.
(114) Silva-Junior, M. R.; Schreiber, M.; Sauer, S. P. A.; Thiel, W. Benchmarks for electronically excited states: Time-dependent density functional theory and density functional theory based multireference configuration interaction. *J. Chem. Phys.* **2008**, *129*, 104103.
(115) Tozer, D. J.; Peach, M. J. G. Molecular excited states from the SCAN functional. *Mol. Phys.* **2018**, *116*, 1504−1511.
(116) Perdew, J. P.; Chowdhury, S. T. u. R.; Shahi, C.; Kaplan, A. D.; Song, D.; Bylaska, E. J. Symmetry Breaking with the SCAN Density Functional Describes Strong Correlation in the Singlet Carbon Dimer. *J. Phys. Chem. A* **2023**, *127*, 384−389.
(117) Send, R.; Kühn, M.; Furche, F. Assessing Excited State Methods by Adiabatic Excitation Energies. *J. Chem. Theory Comput.* **2011**, *7*, 2376−2386.
(118) Janesko, B. G. Rung 3.5 density functionals: Another step on Jacob's ladder. *Int. J. Quantum Chem.* **2013**, *113*, 83−88.
(119) Arbuznikov, A. V.; Kaupp, M. Localized hybrid exchange-correlation potentials for Kohn−Sham DFT calculations of NMR and EPR parameters. *Int. J. Quantum Chem.* **2005**, *104*, 261−271.
(120) Arbuznikov, A. V.; Kaupp, M.; Bahmann, H. From local hybrid functionals to "localized local hybrid" potentials: Formalism and thermochemical tests. *J. Chem. Phys.* **2006**, *124*, 204102.
(121) Holzer, C. An improved seminumerical Coulomb and exchange algorithm for properties and excited states in modern density functional theory. *J. Chem. Phys.* **2020**, *153*, 184115.

https://doi.org/10.1021/acs.jpca.4c02852
J. Phys. Chem. A 2024, 128, 6046−6060